An altimetry based examination of the path and variability of the Agulhas Return Current.

Yotam Fadida

FDDYOT001

Supervisors: A/Prof Juliet Hermes (UCT), Dr. Neil Malan (SAEON)

A minor dissertation submitted in partial fulfilment of the requirements for the degree of Master of Science of the University of Cape Town

Declaration

I know that plagiarism is wrong. Plagiarism is to use another's work and pretend that it is one's own. I have used a Harvard-like convention for citation and referencing. Each contribution to, and quotation in, this minor thesis from the work(s) of other people has been attributed, and has been cited and referenced. This minor thesis is my own work. I have not allowed, and will not allow, anyone to copy my work with the intention of passing it off as his or her own work.

Signed: Yotam Fadida Signed by candidate

Date: 14 December 2018

Abstract

As a result of climate change, partially driven by anthropogenic activity, strengthening wind stress over the worlds oceans is yielding a western boundary intensification and pole-ward shift of oceanic currents (Yang, 2016). Shifting wind regimes and perturbations in neighboring currents have been associated with variations in the flow path of western boundary currents (WBC) and their extensions (Talley, 2011; Combes and Matano, 2014; Nakamura and Kazmin 2003). WBCs, typically characterised by fast flowing and warm currents, are key regions of heat and salt transport as well as for oceanic carbon uptake, air-sea heat flux and nutrient transport, thus positional shifts may have far-reaching implications (Gray and Palter, 2017). While meridional trends (latitudinal migrations) have been observed in analogous WBCs and their extensions, no long-term investigation (decadal) into the flow path and position of the Agulhas Return Current (ARC) has been carried out. Now, with over 25 years of altimetric, satellite remote observation data available, a better understanding of the flow path, seasonal cycle, meridional trends and eddy kinetic energy (EKE) of the ARC is possible.

Here we provide a detailed description of the flow path of the ARC together with several mechanisms that may be contributing to the current's apparent stability. In addition we demonstrate that the documented western boundary intensification and pole-ward shift may be manifesting itself in two ways in the ARC, an increase in regional EKE and a southward trend found mainly in the flow-path of the eastern section of the ARC.

Our results show a strong link between the EKE of the region and the Subtropical Indian Ocean Dipole, both of which are associated with the Southern Annular Mode (SAM), illustrating the effects that southward shifts in the subtropical high pressure system have on regional and mesoscale climate modes.

The combination of a stable, topographically forced flow path with observed EKE increases, demonstrate the effects of wind stress intensification on a region highly influenced by its bathymetry.

Further research into the effects of enhanced eddy activity is necessary, as it has been shown to affect regional primary production (Falkowski, 1991; Oschlies, 1998) and air-sea interactions, thus having potential ramifications for regional aquaculture, weather and fisheries, as well as calculations/models concerned with heat-flux and carbon exchange.

Acknowledgements

I must thank A/Prof Juliet Hermes for all of the encouragement, help, advise and support throughout this work. For pushing me to try new directions, explore new ideas and meet with other proffesionals in the field. Your help has made this period significantly easier, more productive and enjoyable. The quick responses, experience and insights proved invaluable.

I would also like to thank Dr. Neil Malan for all of the guidance and support through these past months. Always willing to help with enthusiasm and a fresh cheerful attitude, your input, views and interesting ideas were crucial in this thesis. Thank you also for all of the assistance with the coding portion of the project.

I thank Dr. Julie Deshayes for challenging me to always try to improve my research techniques and for providing important advice and ideas.

I acknowledge the funding received from the South African Environmental Observation Network (SAEON).

A big thank you to my familiy back home for tons of support and love and especially to the wonderful Neta Peled who stood beside me selflessly and encouraged me throughout these trying times.

Contents

1.Introduction

After flowing pole-wards along the southeast African coast line, the Agulhas Current retroflects with a small portion of the current feeding the South Atlantic in the form of Agulhas rings and filaments while the majority of the current, the Agulhas Return Current (ARC), turns east to re-join the South Indian subtropical gyre (Lutjeharms and Ansorge, 2001). The Agulhas Return Current initiates at approximately 26° E and has a meridional position that varies from 36°-42° S. The termination of the current is between 60°-70° E varying between studies (Lutjeharms and Ansorge, 2001; Boebel et al. 2003; Ffield et al. 1997).

The ARC is the east-ward flowing section of one of the five western boundary current (WBC) systems and is thus considered a WBC extension. The importance of these narrow, intense currents, which transport water and energy pole-ward from the warm equatorial regions to the higher latitudes is due, in part, to these regions having the highest values for mean velocity, eddy kinetic energy, air-sea heat flux, and nutrient transport (Dong and Kelly 2003; Frihe et al. 1991; Wu et al. 2012). These areas are characterized with having vast air-sea interactions due to the presence of strong SST gradients along the current (Small et al. 2008). These interactions have significant impacts on both regional and global climate systems which leads to these currents having a large influence on regional weather, fishing industries and shipping routes. In addition, WBCs have a major role in the global carbon cycle (DiNezio et al. 2009). Due to the fact that they flow pole-wards and slowly lose heat to the atmosphere, these regions generally act as a CO2 sink, effectively removing atmospheric carbon from the air (Gray and Palter, 2017).

Recent studies (Wu et al. 2012; Beal and Elipot 2016; Kwon and Deser 2007) have shown that as a response to global climate change western boundary currents are intensifying and migrating pole-wards (with the exception of the Gulf Stream). The main mechanism driving this change is thought to be an intensification and pole-ward shift of near-surface ocean winds which is attributed to positive annular mode-like trends (Yang et al. 2016).

Work conducted on the positional variability of other WBC extensions like the Kuroshio Extension and the Gulf Stream have shown these regions are often influenced by neighboring currents, climate modes and wind shifts. The Brazil-Malvinas confluence for example has migrated southwards at a rate of approx. 0.6° per decade between 1992-2007 as a result of a weakening in the Antarctic Circumpolar Current (ACC) which is a result of a weakening of the westerly winds over the Southern Ocean (Combes and Matano 2014). These ocean-atmosphere interactions have been linked to important large scale

climate modes such as the Pacific Decadal Oscillation and the North Atlantic Oscillation (Joyce et al. 2000; Qiu 2003; Kelly and Dong 2007; DiNezio et al. 2009). Furthermore changes and variations in these currents have been correlated to changes in the strength of heat advection in to the atmosphere, further linking the variability of these regions to the carbon cycle (Kwon et al. 2007). While several studies have been conducted on other WBC extensions there is a gap in the literature when it comes to the full extent of the ARC.

The objective of this body of work is to assess the positional variability of the ARC over the past 25 years in order to reveal any emerging patterns or trends. In addition the EKE of the region will be examined in order to investigate possible impacts and implications of the WBC intensification trend.

In this thesis we explore several aspects of the ARC by utilizing 25 years worth of reprocessed altimetry data, combining satellite observations with float and ship based measurements. Novel methods were developed for the purpose of describing the exact path along which the ARC flows based on SSH gradients. Other aspects that were examined include meridional variability, meridional trends (latitudinal migrations-in this case, pole-wards), bathymetric influences on the current, EKE trends, seasonality and variability.

2. Literature Review

The warming of the oceans is a well documented phenomenon which is due, to a certain extent, to anthropogenic green house forcing (Levitus et al. 2001). The temperature rise in the upper layer of the ocean (up to 2000 meters) is particularly large in the subtropics (25°-40°) (Alory et al.2007). As a result, there is much research on the processes that occur in the large-scale circulation at the mid-latitudes in an attempt to determine and assess the effects of global warming on the Earth's climate.

2.1 The Main Oceanic Gyres

The upper layer circulation at the mid-latitudes is characterized by the subtropical ocean gyres consisting of a fast western boundary flow with a slower return flow that is in approximate volume balance (Hall and Bryden, 1982). The shape of this surface circulation is derived mostly from near-surface wind forcing on a basin-scale in each ocean (Huang and Russell 1994). Each of the five subtropical gyres (North and South Atlantic, North and South Pacific and the South Indian) are characterized by a generally anticyclonic flow confined within similar boundaries (Figure 2.1). The western boundaries are fast pole-wards flowing currents : Gulf Stream, Brazil Current Kuroshio, East Australia Current, and the Agulhas Current systems. The eastern boundary current regimes of these anticyclonic gyres are, respectively : Canary Current, Benguela Current System, The California Current system, Peru-Chile Current System and the Leeuwin Current which all flow equator-wards with the exception of the Leeuwin which flows pole-wards. (Talley et al 2011).

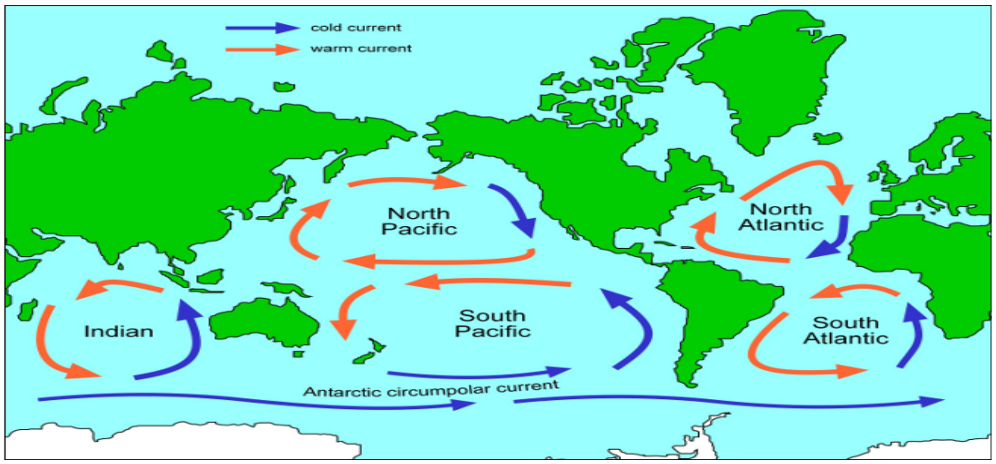

Figure 2.1 An illustration of the location and circulation of the five main oceanic gyres. The red arrows represent the path of the warm pole-ward flowing WBCs and the blue lines represent the cool equator-wards flowing eastern boundary currents (Science Learning Hub – Pokapū Akoranga Pūtaiao, University of Waikato, www.sciencelearn.org.nz).

The subtropical gyre's eastern and western fringes have strong horizontal gradients of temperature (T) and salinity (S) resulting in a deep pycnocline at their centers which are generally vertically and horizontally stable.

2.2 The South Indian Ocean Gyre

The flow in the subtropical South Indian Ocean Gyre (SIOG) is stronger than that in the South Atlantic or the South Pacific gyres. In addition the shape of the circulation in the SIOG is rather rectangular in comparison to the triangular shape of the circulation in the South Atlantic. The majority of the volume transport occurs in the western and central regions of the basin. The east-wards flowing portion of the circulation begins at the Agulhas Retroflection, feeding the Agulhas Return Current (ARC) with approximately 60 Sv. A third of that volume recirculates in a south-western Indian subgyre, refeeding the Agulhas Current, while another third diverges northward between 60°-70° E, terminating the ARC. The remaining 20 Sv split in to two halves before reaching the west coast of Australia, with roughly 10 Sv flowing north to rejoin the west-ward flow and the rest turning south resulting in a net southward transport of 10 Sv from the South Indian Ocean into the Southern Ocean (Stramma et al. 1997).

Changes regarding the volume transport in the SIOG have been documented in a number of studies, most notably in a paper by Palmer, Bryden and Hirschi et al. (2004). A west-ward shift in the point of maximum south-ward transport was reported along with an estimated 40% overall increase in the gyre transport between the years 1987-2002. Further more, 20th century climate simulations from the IPCC AR4 models indicate that a 0.5° south-ward shift in the location of the SIOG is related to the strengthening of the westerly winds. This positional shift has been associated to an upward (positive) trend in the Southern Annular Mode Index (SAM). (Alroy et al. 2007). This variability in the position, transport volumes and temperatures in the Indian Ocean has major climatological implications. Experiments conducted with an atmospheric general circulation model suggest that the rising temperatures in the Indian Ocean played a role in the drying trend between 1950-1990 in the region of West Sahel, a transitional zone in Africa between the Sahara and the Sudanese Savannah (Bader et al. 2003). The results from these experiments also suggested that these rising temperatures may have contributed to a strengthening of the North Atlantic Oscillation (NAO).

The Subtropical Indian Ocean Dipole (SIOD) is an inter-annual dipole coinciding with the austral summer. Positive phases of this dipole are characterized by cold SST anomalies in the eastern region of the Indian Ocean and warm SST anomalies in the west, south of Madagascar (Figure 2.2). This

phase has been associated with increased rain-fall over south-central Africa (Behara and Yamagata, 2001). The formation of the SIOD has been attributed in part to south-ward shifts in the subtropical high pressure system. The subtropical dipole mode in the Indian Ocean often occurs during similar dipole mode events in the subtropical southern Atlantic (Hermes and Reason 2004) and Pacific Oceans (Fauchereau et al. 2003).

The SIOD is also known to affect the seasonal ocean-atmosphere gas exchanges in the southern Indian Ocean. Recent research suggests that SST anomalies related to IOSD in the western Indian Ocean are responsible for decreasing the oceanic CO2 uptake (Metzl et al. 2006; Jabaud-Jan et al. 2004).

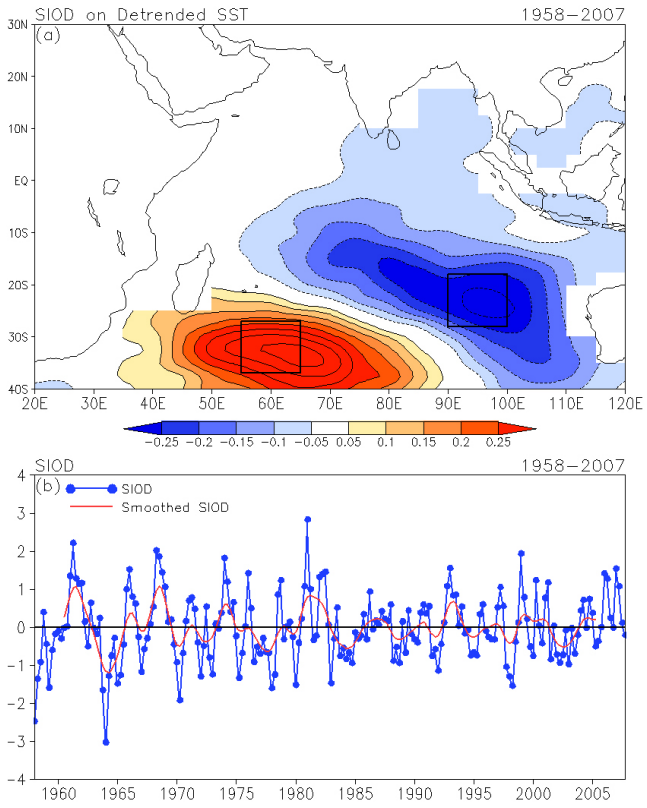

Figure 2.2.(a) The regressed SIOD Index over detrended Sea Surface Temperature (SST) (1958-2007). The western and eastern boxs used to calculate SIOD Index are indicated.. (b)The normalized SIOD index during 1958-2007. The values are normalized by standard deviation of 0.65. Blue line indicates the original time series and the red curve are after applying 1-2-1 smoothing by ten times. (Yjzhao 2011)

2.3 Western Boundary Currents

Western boundary currents are among the regions that hold the strongest SST gradients, with differences of up to of 2° C per 10 km (Friehe 1991). The net surface heat flux mean and variance

at inter-annual and longer time scales is the highest in these regions when compared to the entire global ocean (Wallace and Hobbs 2006). WBCs bring warm water from the equatorial region pole-wards while venting moisture and large amounts of heat along their paths through the mid-latitudes. This redistribution of heat has a massive effect on mid-latitude storms, oceanic carbon uptake and atmospheric jet streams. It has been theorized (Wu et al. 2012) that global warming could have a intensified effect on these highly energetic currents although testing and demonstrating this theory has proved to be difficult due to low amounts of observations.

As a result of the cooling process these currents go through on the path from the warm low latitudes to the cold high latitudes, WBCs and their extensions have a large role in the carbon cycle (DiNezio et al. 2009). The air-sea carbon fluxes are controlled by the difference between the partial pressure of CO_2 in the atmosphere (Figure 2.3), which has been steadily increasing due to anthropogenic activity, and the partial pressure of CO_2 in seawater (pCO_2) (Wu et al. 2012). The cooling of the ocean in the mid-latitudes creates the largest heat-flux in the global oceans and leads to a lower pCO_2 which enables the ocean to absorb more carbon from the air. Thus the WBC regions are effectively acting as ocean sink regions for CO_2 (Gray et al. 2017).

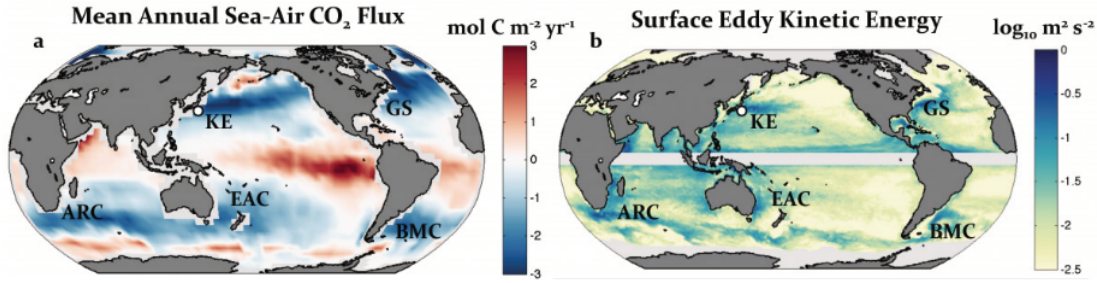

Figure 2.3 Mean annual sea-air CO2 flux for the year 2000 adapted from Takahashi et al. 2009. Blue areas are ocean sink regions for atmospheric CO2 and red areas are ocean source regions (a). Surface eddy kinetic energy calculated for 2011-2013 (b) (Gray et al. 2017).

Reconstruction of century old data sets of oceanic temperatures has shown that the ocean surface warming rate has increased over western boundary currents 2-3 times faster than it has over the global mean ocean surface. Eight different data sets were used for this analysis and although the magnitude of the trend varied between them, from 0.8° C to 1.8° C per century, they all showed a clear warming trend over every western boundary current and their respective extensions. Additionally WBCs (with the exception of the GS) appear to migrating pole-wards as a response to the rising SST. Analysis

conducted with the use of satellite observations, reanalysis products and climate model outputs from the fifth phase of the Climate Model Inter comparison Project (CMIP5) have shown an intensification and pole-ward shift as a long-term global warming effect (Figure 2.4). The cause for this is theorized to be an intensification and pole-ward shift in near surface winds (Yang et al. 2016).

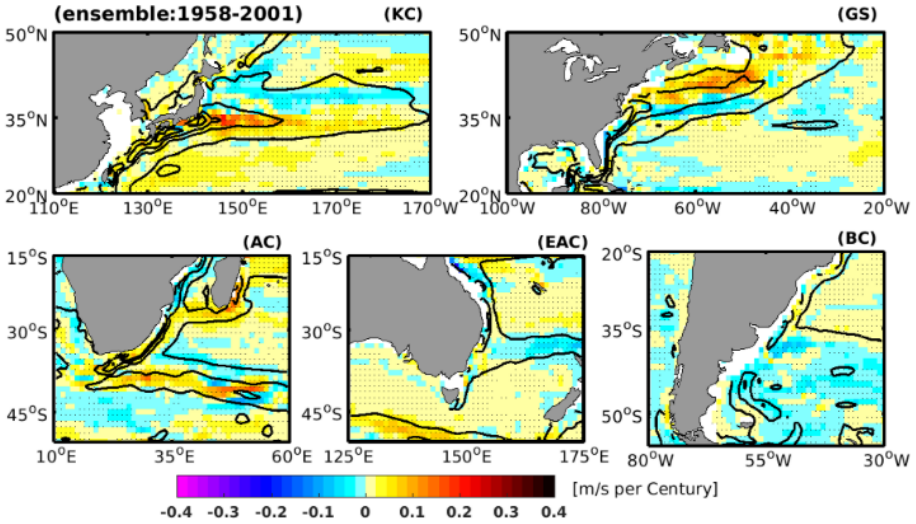

Figure 2.4. Upper ocean (100 m) velocity trends (shading) based on SODA, ORA-S4, GECCO, and GECCO2 ocean reanalyses. Contours represent climatological depth-averaged (upper 100 m) sea water velocity. Stippling indicates areas where at least three data sets agree on the sign of the trends. (Yang 2016)

A systematic change in wind flow strength over both hemispheres, along with an intensification of subtropical WBCs has been associated to the accelerated warming and it has implied that this may lead to a reduced ability for carbon absorption over these regions (Wu et al. 2012). One of the effects of the increased warming in WBC regions was demonstrated through model simulations conducted by Latif and Barnett in 1994 and 1996 respectively. They showed that warm temperature anomalies in the KE, which were a result of increased advection in the KC, lead to reduced SST gradients in the Central North Pacific. This in turn lead to weakened mid-latitude westerlies and a reduced wind stress curl field. As the subtropical North Pacific gyre slowed down, the decreasing heat transport in the Kuroshio reverses the above mentioned event resulting in decadal-scale ocean-atmosphere oscillations (Qio 2003). This observation joins several more in pointing out that although on a large, basin-scale it is the atmosphere that forces the oceanic circulation, on the smaller, mesoscale it seems that the ocean forces the atmosphere (Liu et al. 2007).

Satellite data from the QuikSCAT scatterometer was used to show a positive correlation between near surface wind speeds and SSTs over oceanic fronts and eddies, this is in contrast to a negative cor-

relation that has been noted on basin-scales (Liu et al. 1994). The correlation coefficients between SST and wind-speeds over WBCs were especially high in the southern hemisphere (0.631-0.742) (Minobe et al. 2008). Over the Agulhas Return Current cloud formations were found to differ above warm water and cold water eddies. Thicker and lower clouds (Cloud top pressure of 650mb) were associated with higher SST and higher cloud formations (Cloud top pressure of 570mb) were associated with lower SSTs. In both instances the cloud formations over the ARC region were found to be much higher than the average (Cloud top pressure of 900mb) implying that the interaction between SST and atmosphere reaches higher than the MABL (Liu 2007).

The extent of WBCs influence on regional and global climate regimes is still unclear, however it has been demonstrated that the effects of these current's strong SST gradients are not limited to the MABL. Atmospheric reactions to the temperature front of the Gulf Stream generate surface wind convergences resulting in a localized pattern of precipitation that closely follows the path of the current. The convergence of warm and moist air along the GS path leads to upward motion and to the creation of clouds well into the upper troposphere. An additional factor contributing to this process is that although the magnitudes of wind divergence and wind convergence are similar, the upward motion during surface wind convergence is much stronger than the downward motion during surface wind divergence (Minobe et al. 2008). Since oceanic circulation systems and atmospheric circulation systems are entwined and largely dependent one on the other, it is intuitive to assume that climatological modes are not only influenced by WBCs but also influence the position, strength and thermal content of these currents.

The subarctic frontal zones (SAFZ) correspond to the boundaries of both the sub-polar gyres and the subtropical gyres, displacement of these boundaries results in high SST anomalies. Between the years 1970 and 1985 a 2° southward shift was observed for the SST front of the Pacific SAFZ from 42.5° N to 40.5° N resulting in a regional decrease of approximately 2° C along the Kuroshio Extension front (Nakamura and Kazmin 2003). A 50 year hind-cast analysis with an oceanic global circulation model (OGCM) indicated that a southward shift in the Kuroshio Current resulted in a cooling trend in the Kuroshio Extension during the mid 1980s (Deser et al. 1999). The OGCM hind-cast along with satellite altimeter observations lead researches to believe that much of the SSH variability in the Kuroshio region can be explained by two modes. A southward shift and acceleration in the KE jet during 1976/77 that has been associated to a basin scale wind shift. The second mode reflects decadal variations in the intensity of the KE jet (Taguchi et al. 2007). Similarly, as a result of the strengthening

of the North Atlantic Oscillation, axial shifts in the Gulf Stream occur, inducing meridional incursions reaching 100-200 km farther northwards in the 1990s than in the 1960s (Joyce et al. 2000). The GS tends to reach farther to the north during positive phases of the NAO and shifts to the south during years with increased volume flow through the deep western boundary current (Dong and Kelly 2007; Pen˜a-Molino and Joyce 2008).

It is evident that the variability in the WBC's general paths and positions have far fetching effects on regional and basin-scale climate modes. Even changes on a mesoscale are important when considering the influences these regions have on oceanic circulation and air-sea interactions. The Brazil/Malvinas Confluence (BMC), the meeting point between the pole-wards flowing Brazil Current and the equator-wards flowing Malvinas Current, is usually located near 38° S. Periodic variations in the BMC location have been linked to wind-stress curl variability over the sub-tropical gyre and changes in the ACC transport at the Drake Passage (Matano et al 1993). SSH and SST data from satellites have revealed that besides from these periodic fluctuations, the BMC has drifted south in the period between 1993 and 2008. The magnitude of the south-ward drift varies from 0.81°/decade to 0.39° /decade depending on whether the SSH or SST is used for the calculation (Goni et al. 2011). This observation has been confirmed with the use of surface drifters and along-track satellite data showing a south-wards drift of 0.64±0.20°/decade for the BMC between the years 1992-2007 (Lumpkin and Garzoli 2011). A high-resolution model used to study this event has demonstrated that this south-ward drift is a result of a weakening in the ACC which is a result of a weakening of the westerly winds over the Southern Ocean (Combes and Matano 2014).

Although climate models indicate to the presence of an ongoing pole-ward expansion and intensification of the global winds, which in theory would lead to intensification and pole-ward migration of WBCs, observations show that the Agulhas Current has not intensified since the early 1990s. Rather then an increased mean flow, the strengthening of the winds has increased the eddy kinetic energy, effectively broadening the current due to the eddy activity. Studies conducted in the KC and East Australia current (Yan et al. 2015; Cetina-Herdia et al. 2014) have produced similar results implying that perhaps instead of looking at additional heat being transport pole-wards via intensified WBC we may be facing a decrease in pole-ward heat transport and an increase in the cross-frontal exchange of nutrients and pollutants between the coastal ocean and the deep ocean (Beal and Ellipot, 2016).

2.4 Agulhas Return Current

It has proven to be difficult to assess SSH fields based on satellite data in regions with strong

quasi-permanent features such as those found in WBCs, however statistical analysis and comparisons between MODAS 2D satellite data, RAFOS float data and ADCPs revealed that in the case of the ARC, satellite SSH data can accurately portray the surface velocity field and the mesoscale features (Boebel and Barron 2003). As a definition for the path of the ARC based upon surface velocities, Boebel and Barron used the maximum gradient in the SSH fields.

The path of the ARC begins its eastward flow at ~25° E with a meridional range of between 36° and 40° S in the region westwards of the Agulhas Plateau. Eastwards from the plateau the current shifts slightly to the south with a range of between 37° to 41° S. A three year average of the ARC's SSH field shows a high level of stability in the region characterized by several relatively stationary meanders, three crests and three troughs (Lutjeharms and Ansorge 2001). These meander's locations were corroborated with the RAFOS float data. Further analysis revealed that the location of these three meanders represents an area with especially high variability, second only to the retroflection region (Boebel, Rossby, Lutjeharms et al. 2003). Another interesting feature noticed in this analysis is that the segments between the crests have faster flowing waters than at the peak of the crests ($>$ 0.5 m/s), this behaviour has been noticed in the GS and the SAC as well (Bower and Rossby 1989; Boebel 1999).

Sediment analysis around the Agulhas Plateau indicates that the circumventing flow of the current along the northern edge of this topographic feature existed as far back as the Eocene era, 35-57 million years ago (Uenzelmann- Neben 2002). The reason for this stability in the ARC meanders has long been speculated since such features do not exist in similar currents like the GS and its extension. Meandering in the GS propagates downstream, changing with the flow (Pena-Molino et al. 2008). This has led researchers to believe that topographic forcing has a big role in defining the ARC's path, acting as a stabilizing feature. However, modeling experiments conducted without detailed topographic features have shown a similar crest forming to the east of the retroflection region implying that there are additional dynamics that contribute to the ARCs apparent stability (Pichevin et al., 1999).

Aside from the bottom topography, one probable contributor to the ARCs stability is the ACC which flows parallel to it and in the same general direction. Recent studies have shown that the ACC is surprisingly resilient to climate change, showing no significant response to wind stress intensification (Boning et al. 2008).

Techniques used for identification of oceanic fronts include using the gradients of subsurface density measured from hydrographic sections, following contours of dynamic topography or a combination of

both. One of the challenges in accomplishing this is that in many places there are no strong currents that can be measured near the frontal position (Chapman, 2014). A recent study in the detection of frontal shifts in the Southern Ocean has used cross-track kinetic energy (CKE) from along-track sea surface height anomalies. Although the CKE can not represent the full eddy kinetic energy since it is computed only at crossover points in the satellites orbit, the shapes of the regions examined along ground tracks were the same, and CKE has a much high spatial resolution of sampling (6.9 km). The results from this study show no significant shifts in the frontal positions across the Southern Ocean (Chambers, 2018).

The location of the ARC, which is bordered by the north by the warm Indian Ocean and by the south by the cool ACC, has strong implications regarding the regional and global heat flux. The SST front is softned as a result of the air-sea heat flux around frontal regions. Due to differences between the north and the south of the current in the mixed layer depth (MLD), frontolysis is greatly affected by seasonality. During the summer, there is an increase in the frontolysis to the south of the current due to a shallower MLD and a decrease to the north where the MLD is deeper (Figure 2.5). The amplified air-sea heat flux on the northern side of the current results in a north-south gradient of surface net heat flux (NHF) existing throughout the year with the SST front being stronger during the summer. (Tozuka and Cronin, 2014, Ohishi et al. 2016).

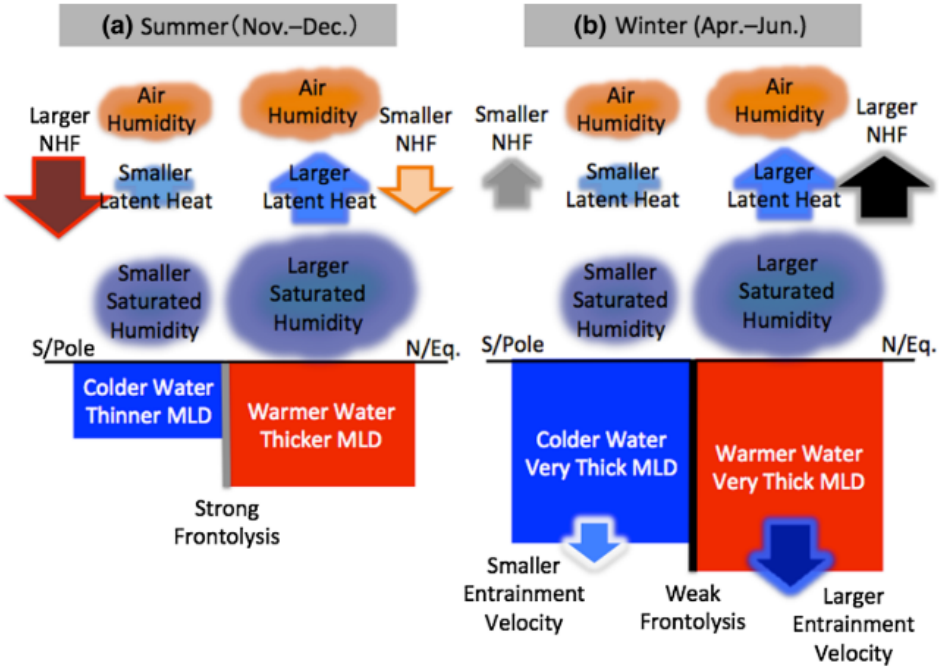

Figure 2.5. Illustration of the mechanisms that drive frontolysis by the NHF and MLD gradient in the summer (a) and

winter (b). (Ohishi, 2016).

The majority of the studies conducted on the ARC are very specific and are usually either temporally or spatially constricted. While the path of the ARC has been described previously in the literature, there is a gap when it comes to longer time scale studies. In addition to the examination of the current over a longer time period, this thesis will investigate the entirety of the ARC region, comparing different sections along the current.

We intend to provide a broader perspective into the ARC, utilizing several data-sets in order to explore the variability of multiple parameters including mean flow path, meridional anomalies and trends, seasonal cycles and EKE. Finally we will link our findings to larger scale climatological modes so as to provide global context.

3.Data and Methods

3.1. Data:

3.1.1. SSH and EKE data

The main product used for this thesis is a gridded, multi-year data set procured through CMEMS (Copernicus Marine Environment Monitoring Service). MULTIOBS_GLO_PHY_REP_015_002 (Link to source-MULTIOBS).

The product is defined as a level 4 product, meaning it is a reprocessed data-set created by combining satellite observations (Sea Level Anomalies, Geostrophic Surface Currents, Sea Surface Temperature) with in-situ observations (Temperature and Salinity profiles). The spatial resolution is 0.25° x 0.25° with a temporal resolution consisting of monthly means spanning over 25 years (1993-2017). The region of observation was restricted in order to isolate the path of the ARC and to make it possible to differentiate between the Agulhas main current, the Retroflection Region and the Return Current. The frame in which calculations and observations were analyzed was 36.125°-46.125° S and 25.125°-70.325° E. This data-set was chosen for several reasons. The combination of remote sensing with in-situ measurments helps provide a more robust and accurate depictment of the region. Additionaly this data-set is one of the only data-sets available that contains 25 years worth of continuously compiled and processed observations. Finally, the spatial and temporal resolutions in the data-set match the scale of the processes that we have chosen to examine.

3.1.2. Oceanic mode indices

In order to identify possible contributors to the variability of the ARC, indices of the major climatological modes were examined. The modes that were included were ENSO (El Nino-Southern Oscillation-Link to source-NINO3.4, Rayner et al. 2002) indexing SST anomalies derived from the HadISST1 global data-set. IOSD (Indian Ocean Subtropical Dipole-Link to source-IOSD, Behara and Yamagata 2001) indexing SST anomalies derived from the HadISST1 global data-set. SAM (Southern Annular Mode-Link to source-SAM, Marshall 2003) indexing sea-level atmospheric pressure anomalies collected by BAS (British Antarctic Survey). AAO (Antarctic Oscillation-Link to source-AAO(CPC AAO index)) indexing 700mb atmospheric anomalies from CPC/NOAA. These indices were procured from KNMI Climate Explorer (Link to source-KNMI link) and all data sets consisted of monthly data for the same time period as the gridded SSH data-set mentioned above.

3.1.3. Bathymetric Data

The bathymetry data-set used was the The GEBCO_2014 Grid, version 20150318 which is a

continuous terrain model for ocean and land with a spatial resolution of 30 arc seconds. The data was procured from GEBCO (General Bathymetric Chart of the Oceans-Link to source-GEBCO data set).

3.2. Methods

The methodology of this thesis is a key component of the research carried out due to the usage of several novel approaches to two main areas, assessing the ARC core\path (3.2.1) and estimating the EKE of the ARC region (3.2.4) hence the novel methods utilised are explained in detail.

3.2.1. ARC Core Position

The main objective of this research was to assess whether there has been a significant trend or shift in the ARC path/location in the past 25 years. To do so, identification of the location of the ARC core was the initial focus. The method for calculating the current's core position was based on the method developed by Boebel and Barron (2003) in which they used the maximum gradient within the SSH fields as a proxy for the location of the current. This method was validated by comparing the data they generated to float and ADCP data.

The ARC was divided longitudinally into nine separate sub-regions of 5° each (primarily based on the location of the quasi-permanent features in the western region of the current and decidedly all slices are the same size for the sake of consistency) to determine whether different areas in the current behaves differently. In order to assess the current it was necessary to calculate the maximum SSH gradient in each of these regions, four methods for doing this were evaluated.

The first method simply calculated the gradient along the central longitude for each region i.e. in region 1 (25.125°-30.125° E) the maximum gradient was located along 27.625° E (Figure 3.1a).

The second method was to calculate the maximum gradient found in each region by calculating the gradients along both axis of the matrix and then seeking the highest value. This produced a single point for each of the nine regions that marked the core location of the current in that region (Figure 3.1b).

The third method was to average the the SSH values in each region zonally, producing a single meridional line of SSH values per region. The maximum meridional gradient of the region was then chosen to mark the current core (Figure 3.1c).

The fourth method, on which the majority of the thesis was developed, located and displayed the maximum SSH gradient per each individual longitude within the chosen frame. This method was ultimately chosen since it produces a much clearer representation of the ARC path. It is the only method that provides a clear view into the nature of the quasi-stationary meanders and into the

precise locations at which the current path shifts in direction (Figure 3.1d).

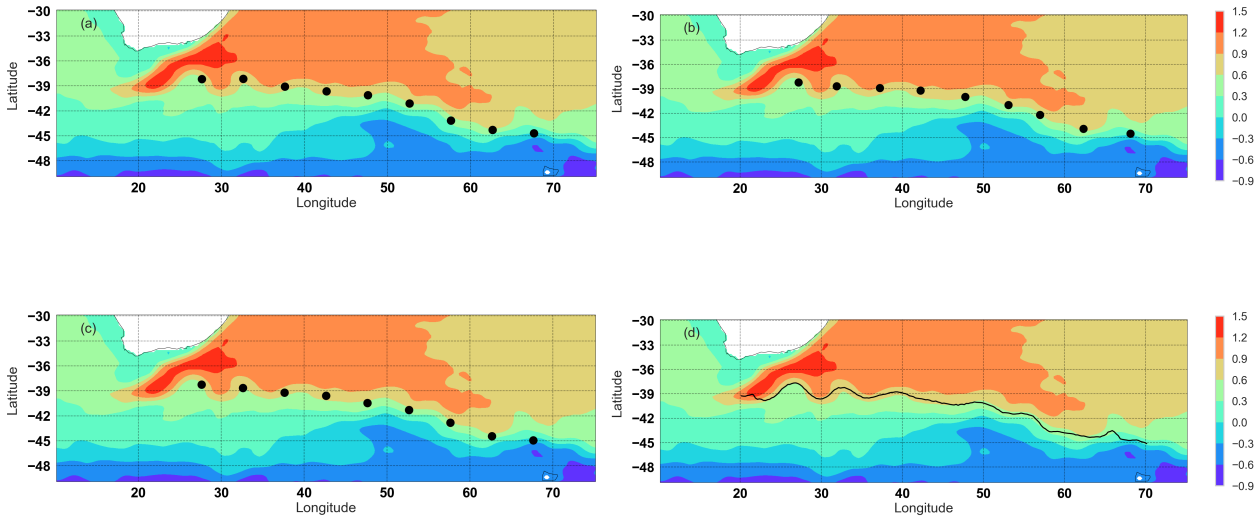

Figure 3.1. The mean SSH (m) field averaged from 1993-2017. Overlain is the ARC mean path (25 years) as calculated using four different methods: (a) Maximum SSH gradient per central longitude in each slice, (b) Overall maximum SSH gradient per slice, (c) Maximum SSH gradient per slice averaged meridionally, and (d) Maximum SSH gradient per individual longitude in the entire frame. The black dots represent the mean location of the maximum SSH gradient for each slice.

Following the establishment of a reliable method for locating the core of the ARC, mean current positions were calculated for differing temporal resolutions. In order to capture the highest resolution possible, the mean current position was calculated per each individual longitude per month and not for a general region. The data-set used has 298 months on record and therefore provides a robust mean showing the average position and path of the current. Monthly positional means were calculated in order to find a seasonal cycle so that it could then be removed thus providing a clearer view of inter-annual trends and shifts. This was done by removing the mean monthly anomaly from the overall mean.

Aside from creating a time series of the actual current path and position, a general mean current location was calculated by averaging all of the maximum gradient points in the given frame, providing a single latitude as a value per month. This assisted in the identification of inter-annual patterns and trends. The distribution of the mean current location time series was tested with a histogram and a residuals test (Figure 3.2).

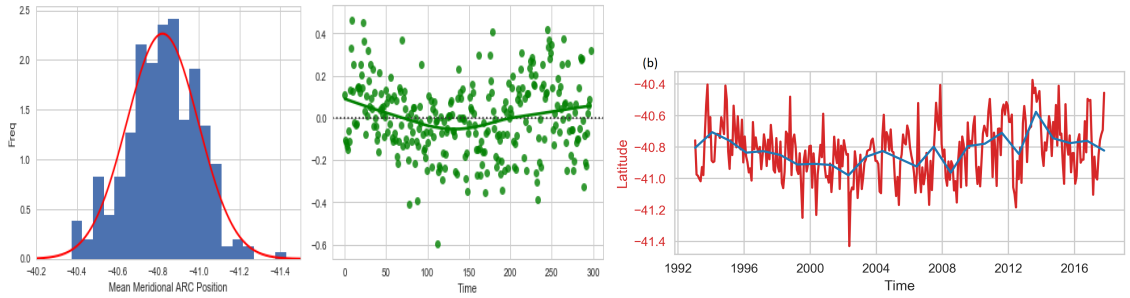

Figure 3.2. A histogram of the mean current location (latitude) per month revealing a normal distribution (Left). A plot of the residuals shows an even spread around the mean meridional position implying normality as well (Center). The mean meridional position of the ARC plotted by time (months in red, annual mean in blue) calculated from the maximum SSH gradient and averaged per month. (Right).

3.2.2 Identifying subregions of the ARC

Anomalies in the mean current location (latitude) were calculated by subtracting the overall 25 year period mean from the monthly/annual means. This was done in order to identify anomalous years that coincided with major oceanic modes likes ENSO, SAM, IOSD etc. This presented a problem since although the mean current position does provide information regarding the general meridional position of the ARC, the region examined is relatively large (≈5550 km) and therefore different sections of the current behave differently. For the investigation of certain parameters the ARC region was split into several sub-regions, western (20°-36.3° E), central (36.3°-52.6° E) and eastern (52.6°-70.1° E). The sub-regions were chosen based partially on bathymetric features and partially on patterns that stood out in meridional position variance and EKE variance calculations.

The ARC was examined through two main approaches, the first was by considering the mean latitudinal position of the current (Latitude by month), both as one complete system and as the sub-regions mentioned above (Figure 4.5). The second approach was to examine each individual longitude in the frame and to create an associated time-series (consisting of latitude with maximum gradient by month). This allowed us to view the temporally based trends in a clear spatial context (Figure s 4.7b, 4.8).

Trends and variability were calculated per longitude in order to demonstrate how different parts of the current behave differently. Trends were calculated by fitting the current core location per month per each individual longitude into a linear regression formula:

$$m = \frac{\sum_{i=1}^{n}(x_i - \bar{x})(y_i - \bar{y})}{\sum_{i=1}^{n}(x_i - \bar{x})^2}$$

Where m is the slope of the trend in the meridional position of the ARC path, x_i is month i and y_i is the current core latitude at each month i in the n-point time series, $\bar{x}$ and $\bar{y}$ are the average of x_i and y_i respectively.

The positional variability was calculated in a similar manner. Variance of the core current position was calculated per each individual longitude :

$$s^2 = \frac{\sum (X - \bar{X})^2}{N - 1}$$

Where s^2 is the variance of latitude x in the N-point time series (months). $\bar{x}$ is the average latitudinal current position.

Mean current positions for different temporal resolutions were examined starting with a 25 year trend analysis followed by a 5 year and 1 year mean. The reason for this was to gauge whether a seasonal cycle influences the mean current postion and also to see if temporary shifts in the current's location could be associated with major oceanic modes of variability.

Dominant frequency identification was done by applying a spectral density analysis to the time series to identify what part of the signal can be attributed to seasonality and what part can be considered trend.

3.2.3. Bathymetry

After observing that certain characteristics of the current are present in all temporal resolutions, particularly the three meanders at the western section of the current (20°-37° E) and the slight shift to the south after 50° E, the bathymetry of the region was examined in order to seek a possible explanation for the nature of the path. The mean path of the ARC was plotted over the bathymetric map to examine the extent of the correlation between the location of the quasi-stationary features along the current and the regional bathymetric features.

In order to investigate the influence of depth on the ARC path, the depth under each point of the current was plotted along side the mean flow path.

3.2.4. EKE

An additional aspect of the current that was examined was its energy content, particularly the eddy kinetic energy (EKE). Unlike the SSH fields, the EKE was measured meridionally across the current sections. The EKE field was generated by using the v' and u' attributes in the data set, where primes denote deviations from the 25-year time mean, within the formula for calculating EKE:

$$EKE = 0.5(v'^2 + u'^2)$$

Where v' is the horizontal velocity componant and u' is the vertical velocity componant.

Primarily, the EKE was plotted with latitude on the x-axis and EKE (m/s) on the y-axis (Figure 3.3 a), producing the meridional EKE variability. The peaks along the line reflect the eddying nature of the ARC. In order to obtain a value that could represent the over all EKE of the current, the area underneath the line was calculated (by integration) per each individual longitude in the before mentioned frame (201 longitudes) and then summed together. This value does not represent the volume caught under the entire EKE field (Figure 3.3 b), due to the spacing between measurments, but rather it is a sum of the areas underneath each longitudal section (201 longitudes) within the frame thus providing information regarding the energetic content within the entire frame of reference. This allowed us to clearly examine the energetic trends occuring in the region.

The area under each line (longitude) was calculated by integration with the trapezoidal rule method:

$$\int_{x_0}^{x_n} f(x)\,dx = \frac{1}{2}h[(y_0 + y_n) + 2(y_1 + y_2 + \ldots + y_{n-1})]$$

The method was applied to the Simpson's rule of integration and revealed very similar results so all calculations were done with the trapezoidal method.

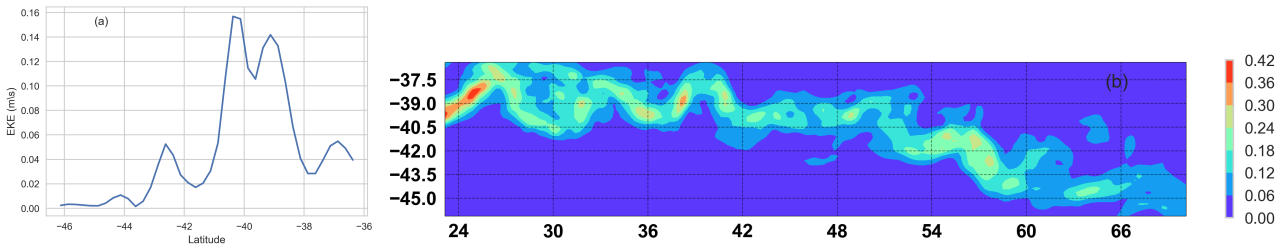

Figure 3.3.(a) EKE (m/s) plotted by Latitude along a single Longitude (30 E) for 1996 . (b) The EKE (m/s) field for 1996 (1996 was chosen randomly to help illustrate the method).

After establishing this method of approximating the EKE content $(m/s)^2$ per month in our defined frame, trends and seasonal cycles were examined. A 25 year time series of the EKE content $(m/s)^2$

was fitted into the linear regression model to provide a slope that represents the regional energetic trend.

The distribution of the EKE content $(m/s)^2$ per month was examined with histograms and residual plots (Figure 3.4), this was done since normality is a prerequisite for using the Pearsons correlation method.

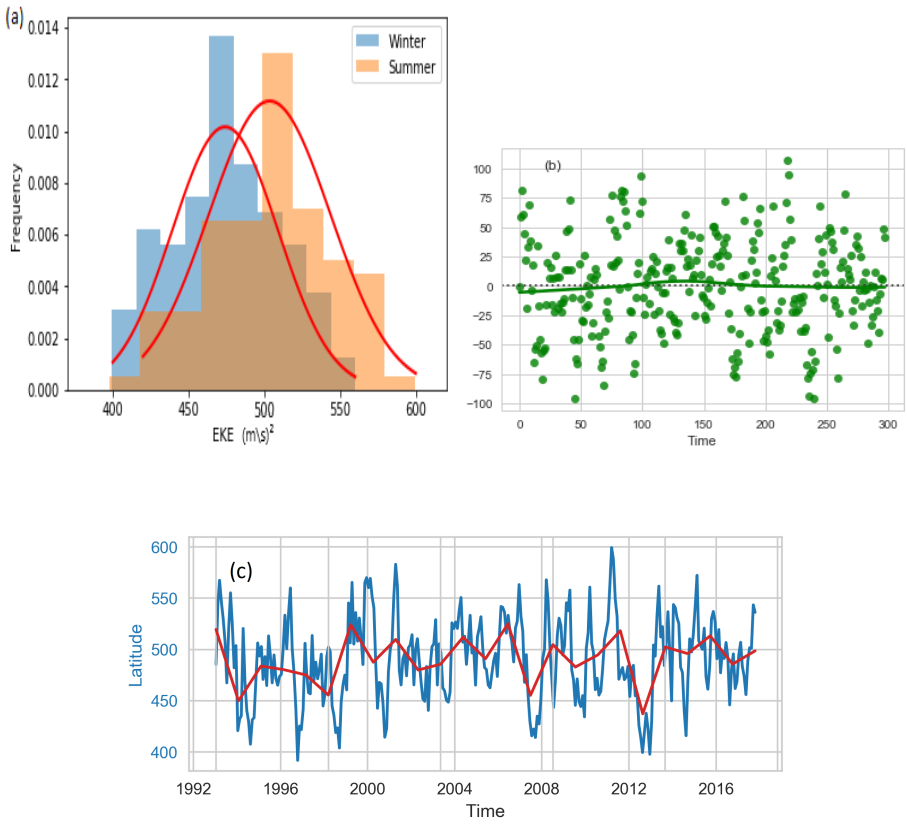

Figure 3.4. (a) A histogram of the regional EKE content $(m/s)^2$ per month. (b) A plot of the residuals shows an even spread around the mean EKE content $(m/s)^2$ imlying normality as well . (c) The regional EKE content plotted by time for the 25 year period (Monthly data in blue and Annual means in red).

In addition to the examination of the overall time period, EKE $(m/s)^2$ was measured in differing temporal resolutions, again, in order to try and correlate the changes to major oceanic modes. Choosing the time frames was done mainly by identifying visualy conspicuous trends from the overall time series (Figure 3.5). Dominant frequency identification was done by applying a spectral density analysis to the time series.

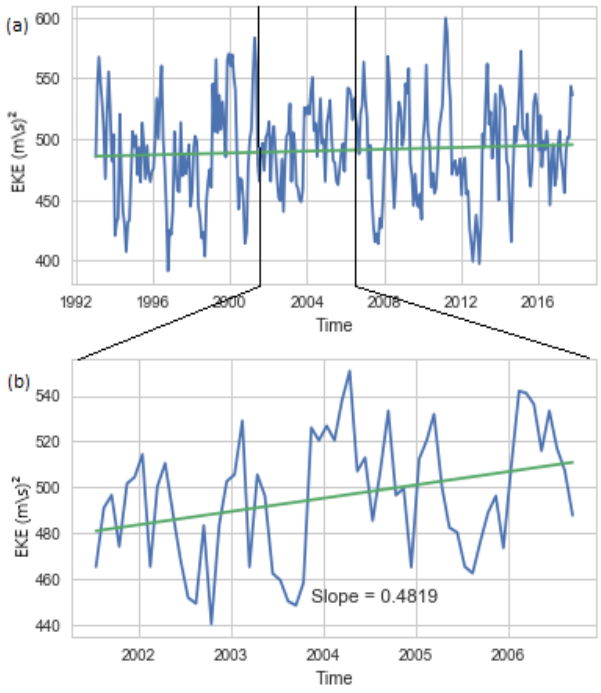

Figure 3.5. (a) Regional EKE content $(m/s)^2$ plotted by time for the whole 25 year time period with (b) an isolation of the years 2001-2006 .

Seasonal effects on the EKE content $(m/s)^2$ were examined by plotting the EKE values per month over the whole time period i.e the EKE content for every January from 1993 to 2017. Additionaly several months were combined to represent the main summer/winter division of the year (January-March for summer, June-August for winter, based on the EKE seasonal cycle literature).

3.2.5. Correlations

In order to investigate probable sources for the variability, both position/path and EKE content $(m/s)^2$, major oceanic modes and events were examined. Primarily the indices for the oceanic modes were plotted over the ARC path/EKE content time series to gauge whether any similarity in the magnitude, general behaviour or direction exists between them. In such cases where similarities were found the Pearsons Correlation method was used to look at the correlation between the series. The significance level for the test was set at α=0.05. Since the data was time dependent, cross correlation was examined over different lags to help find the time gap that produces the highest correlation.

In some cases the monthly data were used for correlation, particularly where seasonal cycles were investigated, for interanual variability examination the anual means were used.

4. Results

4.1. Altimetry

4.1.1 Characterization of the ARC path

The examination of the ARC path over the 25 year time period revealed a relatively high level of positional stability. The current has several quasi-stationary features that stand out at nearly every temporal resolution explored, most notably, a series of meanders at the western-most region of the current (25°-39° E). While there is considerable variability at monthly timescales due to the eddying nature of the current, over scales above the subseasonal, the path of the current is suprisingly stable. The terms used to refer to the meanders in previous studies (Boebel, Rossby and Lutjeharms et al. 2003) and which will be utilized in this chapter for the sake of clarity are C1(Crest 1-27° E) ,C2 (Crest 2-33° E) and C3(Crest 3-39° E) for the meander crests and T1(Trough 1-30° E) and T2 (Trough 2-35° E) for the troughs between the crests. Two additional features that stand out are a south-ward shift in the current path at 55° E which will be refered to as SWS (South-ward Shift) and a small but noticeable meander at 66° E which will be refered to as SC (Small Crest) (Figure 4.1).

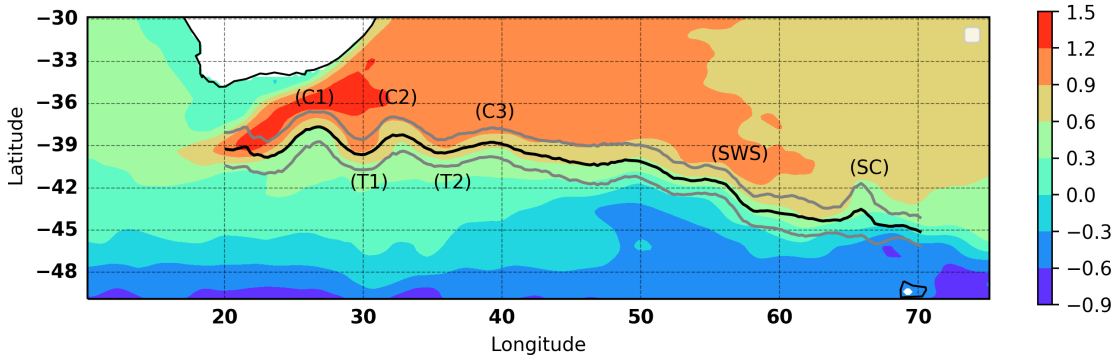

Figure 4.1. The path of the ARC (black) averaged over 25 years as calculated from the maximum SSH gradient with the standard deviation (grey) plotted over the mean SSH field (m). Prominent features marked.

Although the quasi-stationary meanders appear in nearly all of the temporal resoulutions, annual means reveal that there are slight zonal and meridional variations (Figure 4.2). Certain areas within the current tend to display more variability in position than others, thus for the purpose of analysing this tendency the current was divided into sub-regions. The positinal variability of different sub-regions within the ARC will be expanded upon in section 4.5.

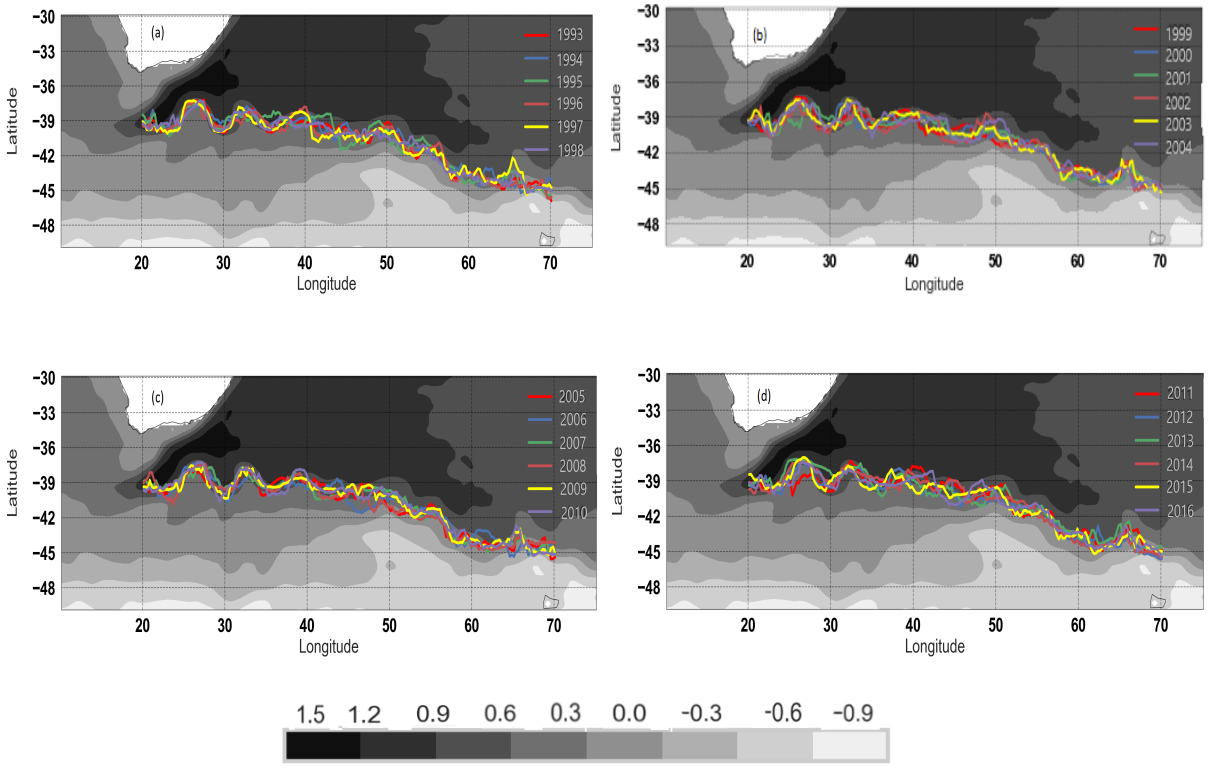

Figure 4.2. ARC path averaged annually for the years (a) 1993-1998, (b) 1999-2004, (c) 2005-2010, (d) 2011-2016, plotted over the mean SSH regional field (m).

4.1.2 Bathymetric Influence

The apparent stability in the location of the ARC meanders is in contrast to analogous WBC extensions such as the Gulf Stream Extension in which the meanders propogate downstream (Pena-Molino et al. 2008). The location and stability of C1 and T1 have been attributed to the presence of the Agulhas Plateau although models simulating the flow of the Agulhas with less detailed bathymetric features have produced a similar feature resembling T1 (Pichevin et al., 1999) thus hinting to the existance of additional contributing dynamics (Boebel et al. 2003). Observations of the path of the mean flow of the ARC plotted over the map of the regional bathymetry (Figure 4.3) suggest a much closer relationship between the locations of the quasi-stationary features and the bathymetric features. All of the features described in section 4.1 appear to be linked to upward and downward slopes along the ocean floor. In a directional sense, while the entirety of the ARC flows generally eastwards, areas in which the current path flows over a bathymetric rise correspond to the path shifting temoprarily northwards. Areas in which the current path flows over a bathymetric valley coincide with the path shifting temoprarily southwards. While the locations of the meanders correspond to

prominent bathymetric features, the magnitude of said features does not seem to affect the magnitude of the meanders.

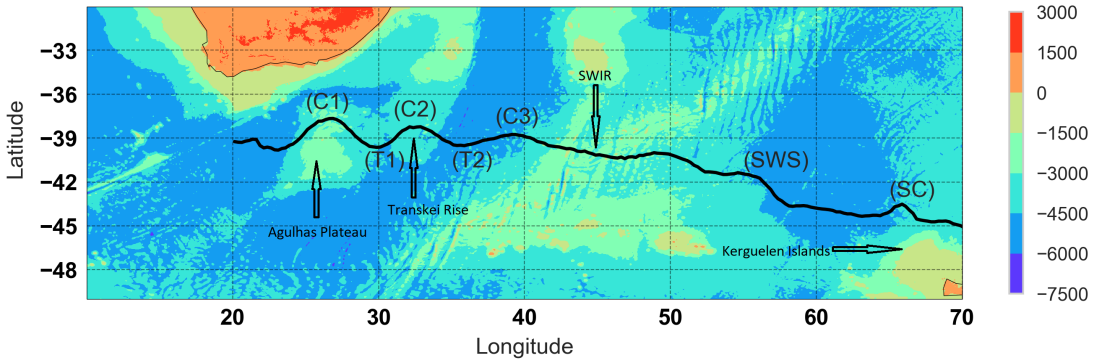

Figure 4.3. The ARC mean path and prominent features plotted over the map of regional bathymetry (m).

The first meander (C1,T1 - 38° S, 27° E) occurs around the Agulhas Plateau followed by the second meander (C2,T2 - 38.5° S, 33° E) which forms over a southern elongation of the Mozambique Plateau named the Transkei rise (Gohl 2011). C3 (39° S, 39° E) appears as the path of the current reaches the western most point of the Southwest Indian Ridge (SWIR) while SWS (42° S, 55° E) corresponds to the deepening at the eastern most point of the SWIR. SC (44° S, 66° E) coincides with a rise surrounding the Kerguelen Islands, the French Southern and Antarctic Lands, in the south Indian Ocean. These observations are in line with the laws of fluid dynamics, particularly the conservation of potential vorticity. The directional shifts react according to the changes of bottom depth as well as the Coriolis component. This concept will be explored further in the discussion section.

4.1.3 Seasonal Variability

The influence of seasonality on the path of the ARC is relatively small compared to interannual differences. There are no large apparent deviations from the mean during either the summer months or the winter months (Figure 4.4 b). The distributions of the mean meridional positions of the ARC during summer and winter (Figure 4.4 a) reveal a 0.05° difference in the mean latitude of the maximum SSH gradient, slightly more to the north during the winter. There is a larger range of latitudinal movement during the winter (0.88°±0.164°) with the distribution completely overlapping that of the summer months range (0.76° ±0.146°). The seasonal variability does not change across the longitude of the current

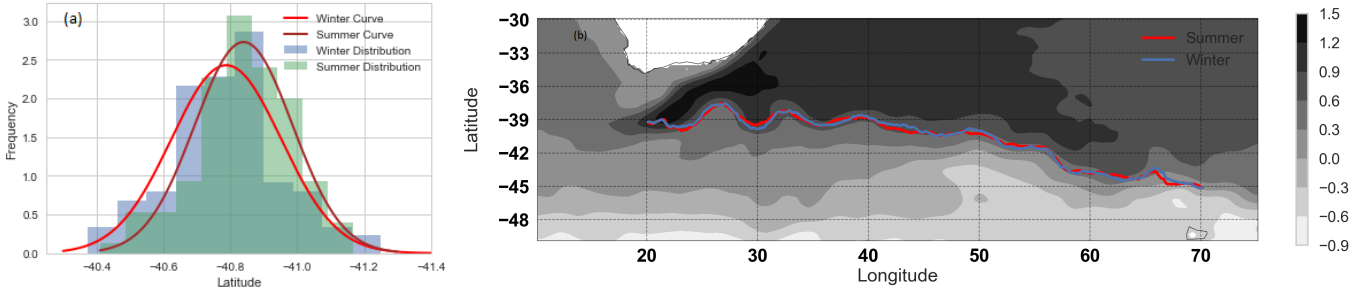

Figure 4.4 (a) A histogram depicting the seasonal distribution of the mean meridional position (Latitude) for the ARC. (b) The mean path of the ARC plotted over the mean SSH field (m) for both summer and winter months.

4.1.4 Anomalies in the ARC Mean Latitudinal Position

Although the features along the ARC path appear to be relatively stable in comparison to other WBC extensions (GS and KE in particular), the monthly meridional deviations from the current's average latitudinal position follow localized trends that last for approximately 5-10 years. While the anomalies are relatively small throughout the majority of the time series, there is a noticeable peak between the years 2012-2016.

There is a slight although significant southward trend (slope=-0.0032, $p<0.05$) in the years 1993-2003 followed by a slight northward trend (slope=0.0037, $p<0.05$) from 2003 to 2013. From 2013 onwards there is a southward trend again until the end of the time series. Different parts of the current follow this pattern to different degrees of magnitude (Figure 4.5). The western region (20°-36.3° E) of the ARC follows this pattern most closely with a linear slope of -0.005 leading to a mean current southward displacement of 0.55° during the first 10 years of the time period. The range of the anomalies in the latitudinal position for this region is 2.13°±0.347° (Figure 4.5b). The middle region of the current (36.3°-52.6° E) follows the pattern to a lower degree with a range of the anomalies for this region is 1.65°±0.333° implying more stability than the western region (Figure 4.5c). The eastern region of the ARC (52.6°-70.1° E) does not appear to follow this pattern, has no notable peaks and has a range of anomalies of 2.10°±0.290° (Figure 4.5d). When observed as one whole system the ARC meridional anomalies are dominated by those that occur in the western section of the current (Figure 4.5a). The diminishment of the temporally localized trends downstream implies that the main contributors to these patterns are found primarily in the western region of the current.

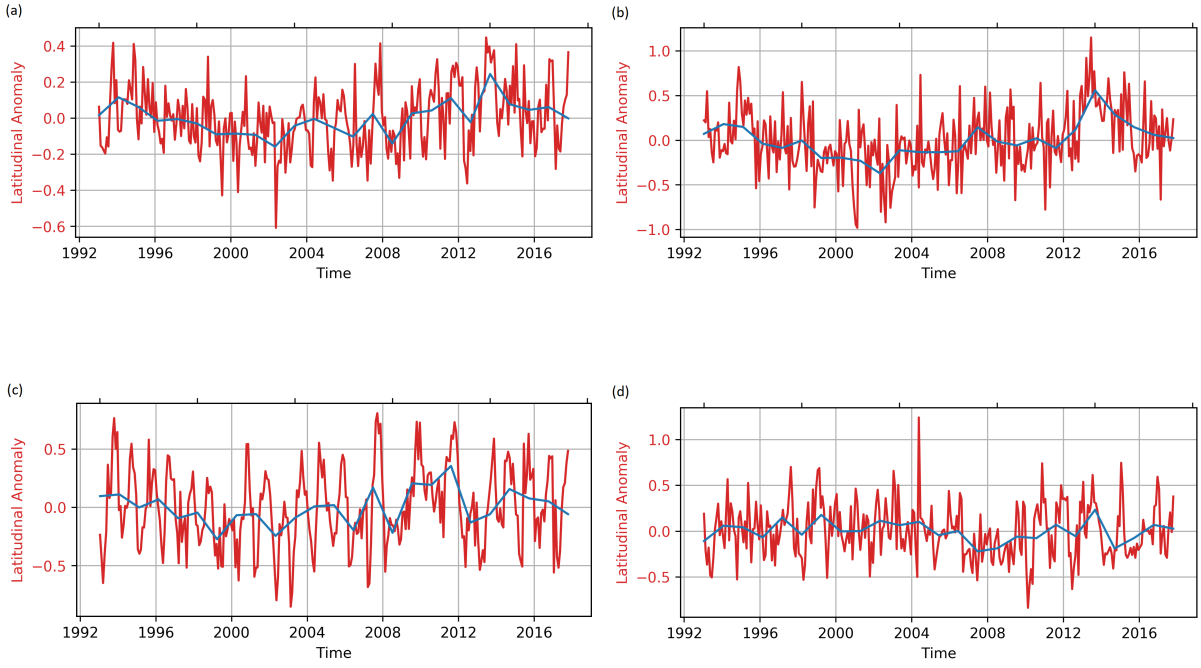

Figure 4.5 The monthly meridional anomalies (degrees) in the ARC path (red) plotted with an annual mean (blue) for different sections of the current. (a) Plotted as one complete system (20-70.1 E) . (b) The western region (20°-36.3° E). (c) The middle region (36.3°-52.6° E) .(d) The eastern region (52.6°-70.1° E).

A power spectral density analysis (cpy) shows the dominant frequency in the time series to be around 5 years (Figure 4.6), in addition the lack of a seasonal cycle (a peak in the semi-anual frequency) is apparent. The reason the peak is not well defined is possibly due to the time-series not being long enough to fully resolve the 5-year periodicity.

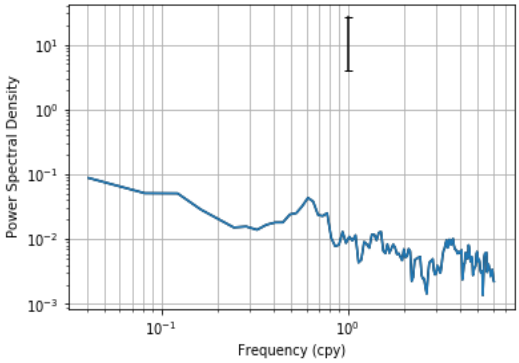

Figure 4.6 A power spectral density analysis of the mean latitudinal postion (cpy) of the ARC (error bar in black).

4.1.5 Variability along the ARC path

The meridional variance of the ARC path varies between regions along the current, much like the other aspects of the current. In contrast to the characterization of the ARC path anomalies, the variability of the current position appears to be less dependent on the zonal division and more closely related to the presence of the quasi-stationary features described in section 4.1 and by association, to the bathymetric properties of the region. The features C1,C2,C3,T1,T2 and SWS are characterized with a low degree of variability while areas linking these features tend to vary more in their meridional position (Figure 4.7), this emphasizes the role of bathymetry in shaping the path of the ARC. The area with the highest degree of variability in the region is SC.

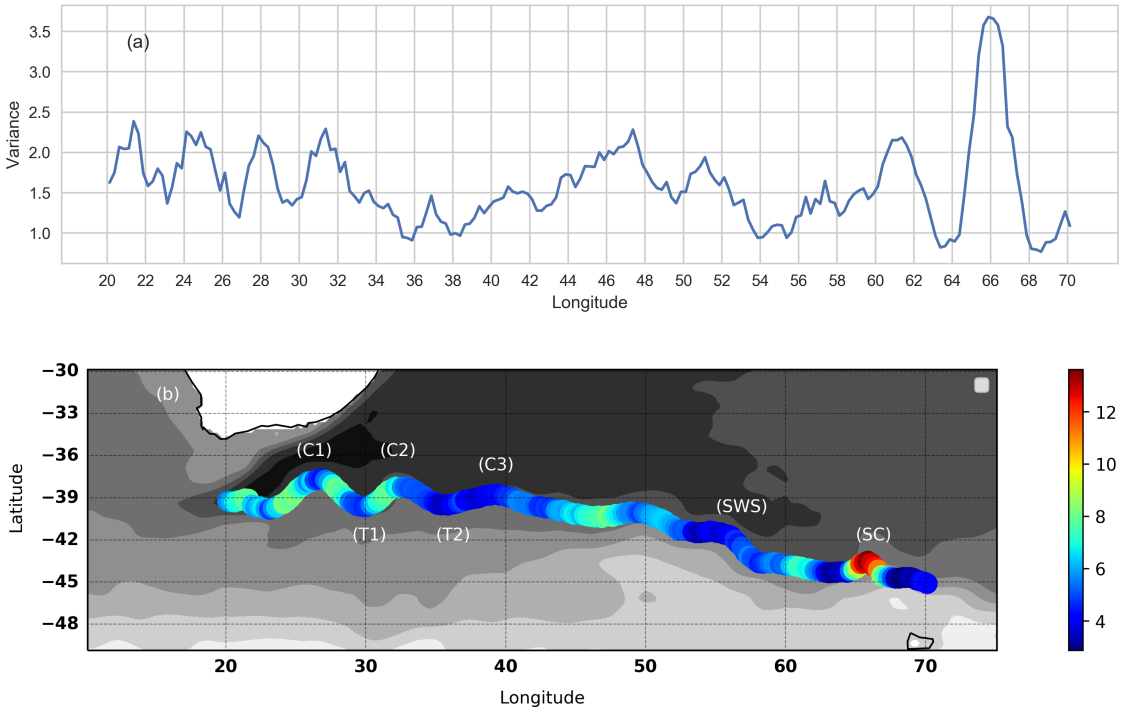

Figure 4.7. Variance (degrees^2) of the meridional component of the ARC path plotted by longitude (a). Variance (degrees^2) of the meridional component of the ARC path plotted in color over the mean SSH field (m) (b).

4.1.6 Trends along the ARC path

The meridional trends along the path of the ARC vary from region to region and do not seem to be linked to the location of the prominent features along the current (Figure 4.8). There is no apparent pattern linking between regional trends to other factors. The magnitude of the trends is relatively small with a maximum northward trend found at location C2 of 0.036°±0.0113° per year and

a maximum southward trend found at 48° E of 0.02°±0.0113° per year. The current eastwards of 47° E is predominantly southbound.

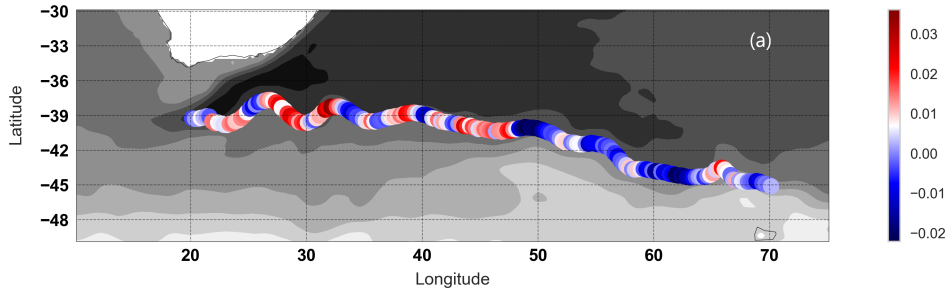

Figure 4.8 The annual meridional trends (degrees/year) per each longitude along the ARC path plotted over the mean SSH field (m).

4.2. Eddy Kinetic Energy

4.2.1 Seasonal Cycle

Unlike the path of the ARC, the bi-modal distribution of the EKE $(m/s)^2$ demonstrates that the region follows a seasonal cycle of higher (lower) kinetic energy levels in the summer (winter) (Figure 4.9). The mean EKE value for the summer months is 503.4±39.27 $(m/s)^2$ with a range of 201.8 $(m/s)^2$. The mean EKE value for the winter months is 474.2±35.75 $(m/s)^2$ with a range of 160.6 $(m/s)^2$. A power spectral density analysis shows that the dominant frequencies found in the regional EKE are annual and semi-annual. There is an additional strong signal for a 7-8 year cycle however the time series is not long enough to allow for significant conclusions to be drawn (Figure 4.10). The month with the highest (lowest) average EKE is February (July) (Figure 4.10.a,b) with velocities of up to 0.5 ms^{-1} (0.3 ms^{-1}).

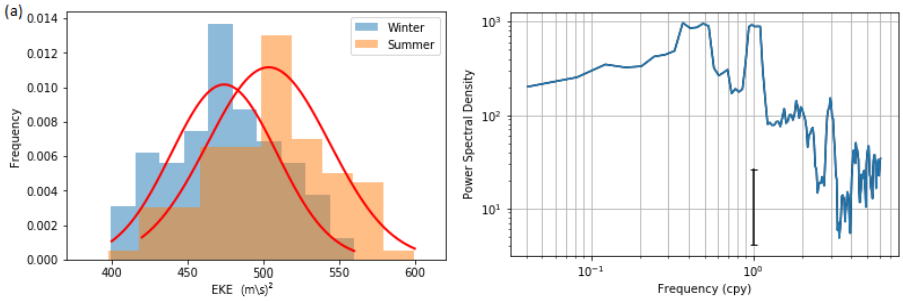

Figure 4.9. (a) A histogram of the summer and winter distributions of EKE $(m/s)^2$ within the defined frame of reference.(b) Spectral power analysis of EKE (cpy) within the defined frame of reference.

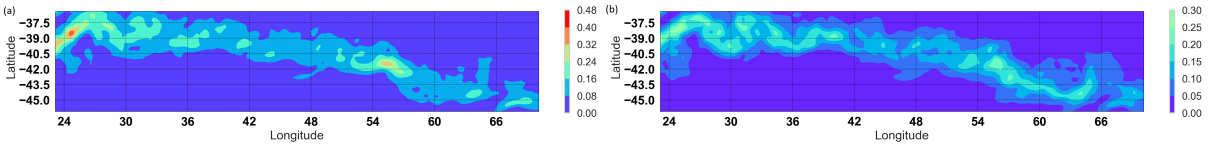

Figure 4.10. The mean EKE (m/s) for February (a) and July (b).

4.2.3 EKE Variability

The EKE variability along the ARC varies with a clear distinction between the western section (24°-40° E), the central section (40°-52° E) and the eastern section (52°-65° E) of the current (Figure 4.11). The western section is characterized with the highest levels of variability with values of up to 0.056 $(m/s)^2$. The central section displays relatively low levels of variability with values of 0.008-0.016 $(m/s)^2$. There is a rise in variability again in the eastern section with values similar to those in the western section but to a lesser spatial extent.

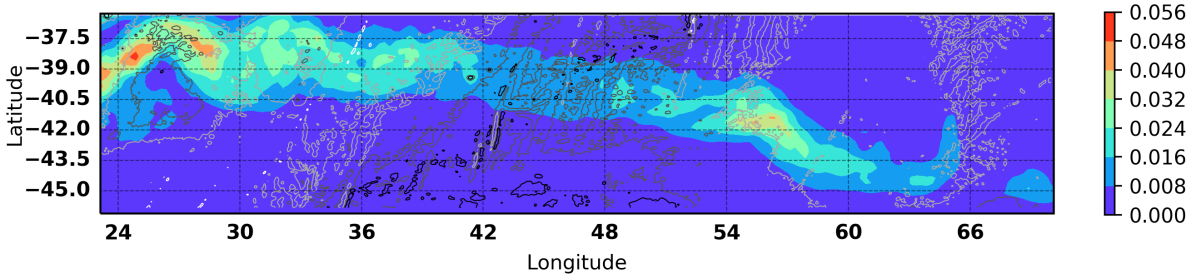

Figure 4.11. The variance $(m/s)^2$ of the EKE in the ARC 1993-2017, contours represent prominent bathymetric features.

4.2.4 Bathymetric Influence

Similarly to the characteristics of the ARC path, the EKE is greatly influenced by the bathymetry of the region (Figure 4.12). Areas with prominent bathymetric features are associated with low levels of EKE. This is most noticeable across the SWIR which has relatively low levels of EKE. The EKE values rise again after the eastern boundary of the ridge only to drop off just before the Kerguelen Islands, producing a shape that resembles the shape of the bathymetric features below the surface.

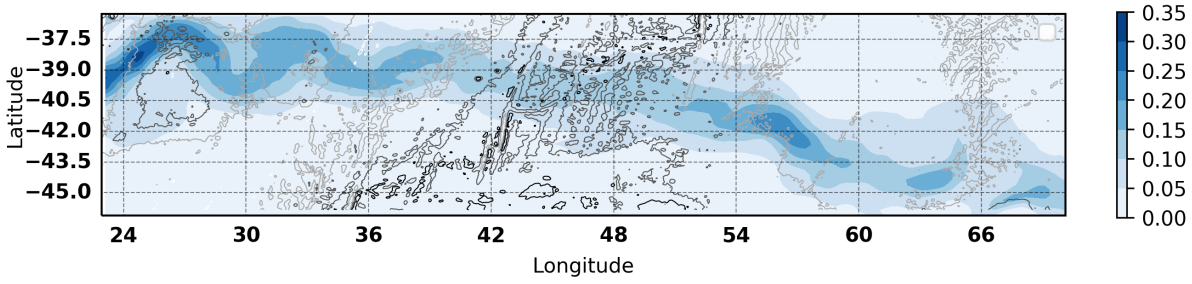

Figure 412. Bathymetric features plotted over the mean EKE (m/s) field.

4.2.5 EKE Trends

The regional EKE time-series reveals an increase in EKE over the past 25 years. The linear trend for the monthly EKE content $(m/s)^2$ is relatively small, 0.032±0.0269 $(m/s)^2$/y (95%, p value= 0.238) and the slope is not significantly different from zero (Figure 4.13.a). The mean EKE values for the summer period (January-March) however show a relatively rapid increase in EKE with a linear trend of 2.221±0.96 $(m/s)^2$/y (95%, p value<0.032) accumulating to an increase of approx. 10% over the past 25 years (Fig4.13.b). The mean EKE values for the winter (June-August) exhibit no significant trend. This relates to the ARC EKE seasonal cycle and its links to several other climate modes, this trend will be further explored in section 4.2.6 and in the discussion section.

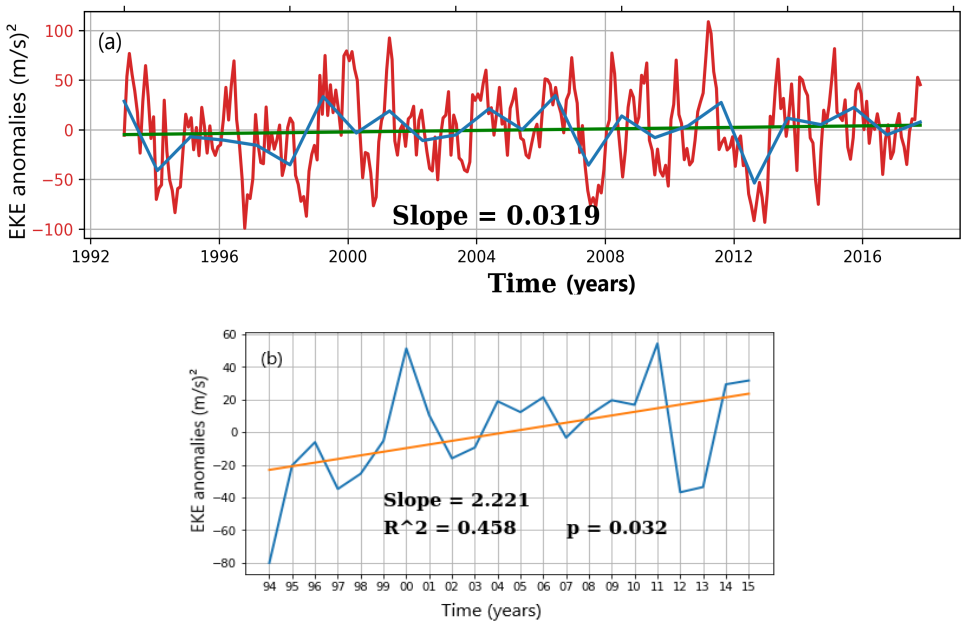

Figure 4.13. Monthly regional EKE anomalies $(m/s)^2$ plotted by time (monthly value in red, annual mean in blue) with the corresponding linear trend line (green) (a). The EKE $(m/s)^2$ anomaly values averaged over the summer months plotted by time with the corresponding linear trend line, r^2 and p value (b).

4.2.6 Links to Climate Modes

Of all the oceanic mode indices examined (see 3.1.2), the two that have the highest correlation to the ARC EKE anomalies are the Southern Annular Mode and the Indian Ocean Subtropical Dipole. The SAM index is based on the zonal pressure difference between the latitudes of 40° S and 65° S and IOSD is based on SST anomalies in the subtropical Indian Ocean. The correlation coefficients vary between different temporal ranges, sometimes reaching high levels of correlation and other times lower levels. When averaged annually the correlation coefficients are at their highest. The correlation between the ARC EKE anomalies and SAM index (annual means 1993-2017) is r=0.28, p=0.18, r^2=0.08, explaining 8% of the variance (Figure 4.14).

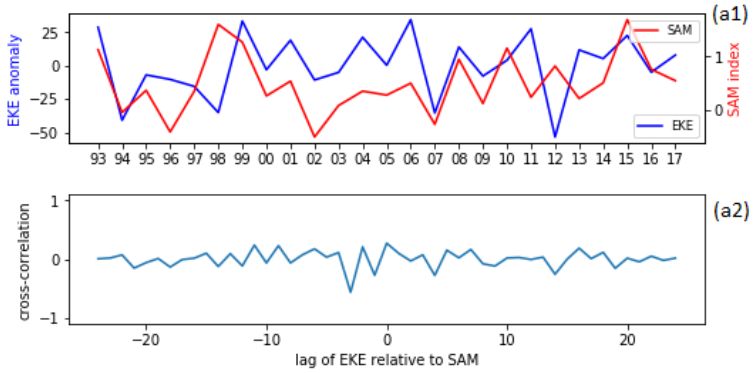

Figure 4.14. The EKE anomalies $(m/s)^2$ plotted over the SAM index for the years 1993-2017 (a). The lag of EKE in relation to SAM (b).

The correlation between the ARC EKE anomalies $(m/s)^2$ and IOSD index (monthly means 1993-2007) is r=0.29, p=8.4e-05, r^2=0.084 (Figure 4.15a). The correlation between the ARC EKE anomalies $(m/s)^2$ and IOSD index (annual means 1993-2007) is r=0.63, (p=0.01), r^2=0.4, explaining 40% of the variance (Figure 4.15b). Between the years 2001-2007 an increase in the correlation between ARC EKE anomalies $(m/s)^2$ and IOSD has been observed, raising the correlation coefficient from r=0.29 to r=0.44, p=2.17e-5 (Figure 4.15c).

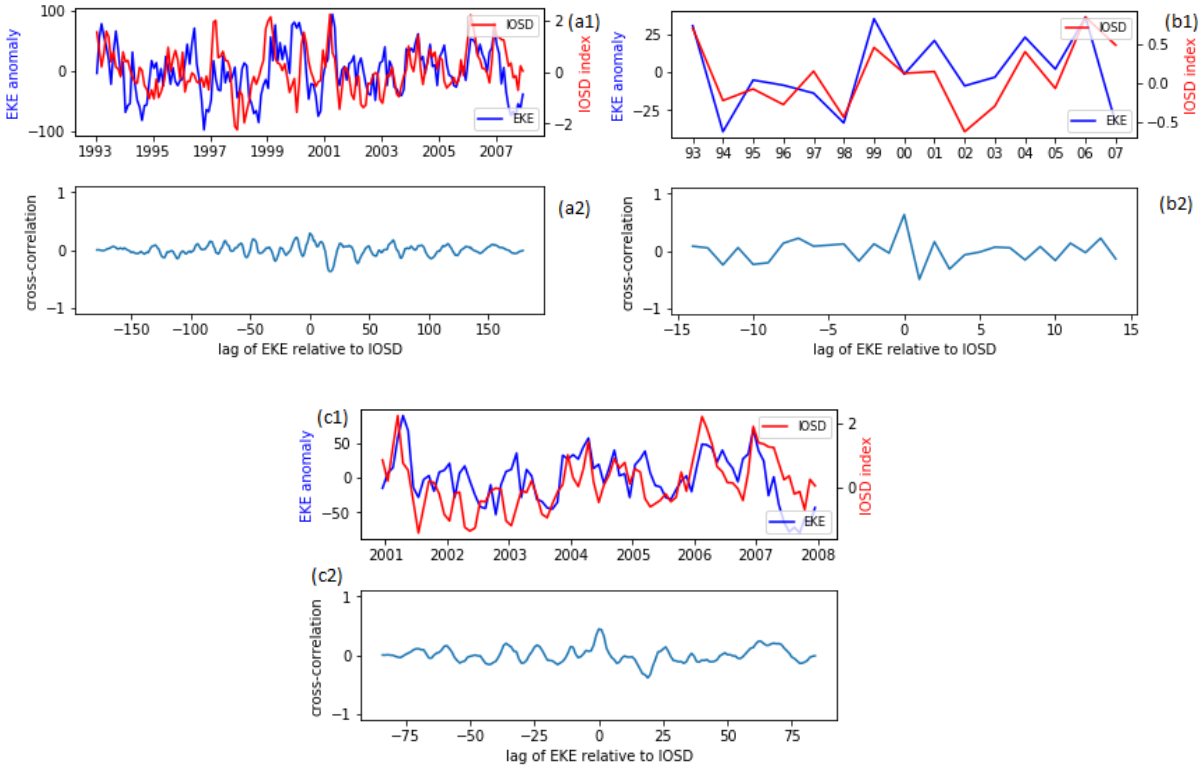

Figure 4.15. The EKE anomalies $(m/s)^2$ plotted over the IOSD index monthly data for the years 1993-2007(a1). The lag of EKE in relation to IOSD (a2). The EKE anomalies $(m/s)^2$ plotted over the IOSD index annual means for the years 1993-2007 (b1). The lag of EKE in relation to IOSD (b2). The EKE anomalies $(m/s)^2$ plotted over the IOSD index monthly data for the years 2001-2007(c1). The lag of EKE in relation to IOSD (c2).

5. Discussion

The primary goal of this work was to examine and assess the path of the ARC based on 25 years of altimetric data in respect to the current location, meridional trends and EKE. Here we explore the mechanisms that drive and shape these characteristics and compare our findings with studies conducted on other WBC extensions.

5.1 The ARC Path

A significant portion of this study revolves around a demonstration of how steady the flow path of the ARC actually is. While during shorter time-scales (weeks-months) the shape of the current is dominated mainly by the formation and transport of mesoscale eddies, when averaged over longer periods, the quasi stationary meanders (Figure 4.1) stand out in an otherwise relatively straight current. In contrast to the meanders in the Gulf Stream and its extension that propagate downstream, the meanders in the ARC appear to be locked in position by one or possibly even several forces. The regional bathymetric features seem to have the most influence on the location and shape of the meanders. A similar example of this phenomenon can be seen in the Kuroshio Current and its extension to the east of Japan. The Kuroshio path has a relatively stable meander that occurs over a rise on the ocean floor (Talley and Delman ,2011) (Figure 5.1).

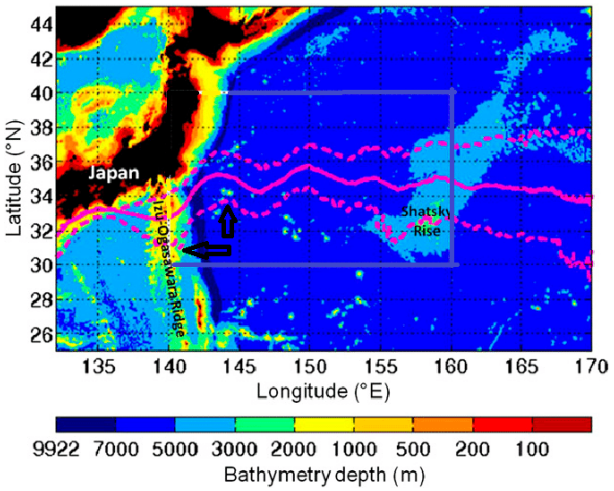

Figure 5.1 Bathymetry in the Kuroshio Extension region. The magenta lines indicate the mean (solid) and 10th/90th percentile (dashed) jet axis positions computed from POP for 1995–2007 (Talley and Delman 2011). Black arrows show bathymetry induced meanders.

The pattern produced is associated with the preservation of potential vorticity (PV) along the flow path of the current. Potential vorticity takes in to consideration not only the local spin (vorticity) but also the height of the water column. Thus if a column is shortened and flattened (preserving mass),

i.e. the path of the current passes over an inclination on the ocean floor, then it must spin more slowly. While the path of the current flows over a declination on the ocean floor the water column is stretched and thinned and should spin faster (Talley and Delman ,2011). The vertical stretching results in the meanders in the ARC shifting counter-clockwise while flowing over an incline in bathymetry and clockwise while flowing over a decline, this can also be described as a topographically forced Rossby wave. The opposite appears to be true regarding the Kuroshio (Delman et al. 2015). This is due to the two currents being located in different hemispheres and therefore the Coriolis effect has opposite effects on the surface vorticity.

While the bottom depth along the path of the current varys greatly (1000-6000 m) the meridional magnitude of the meanders has a smaller range, slowly decreasing as the current flows eastwards. This may be due to the slowly dissipating core of the ARC as it flows eastwards in combination with a weaker influence from PV variations with growing depths. Figure 5.2 illustrates how the varying depths effect the curvature in the flow, changing from cyclonic to anticyclonic and vice versa (the Figure is true for the Northern Hemisphere so the opposite should be applied for the ARC). The column height parameter (h) in the equation is the denominator and there for when the depth increases PV decreases. The average maximum depth of the ARC is between 1000-1500 meters so ΔPV is largest when the bathymetric features are in that range.

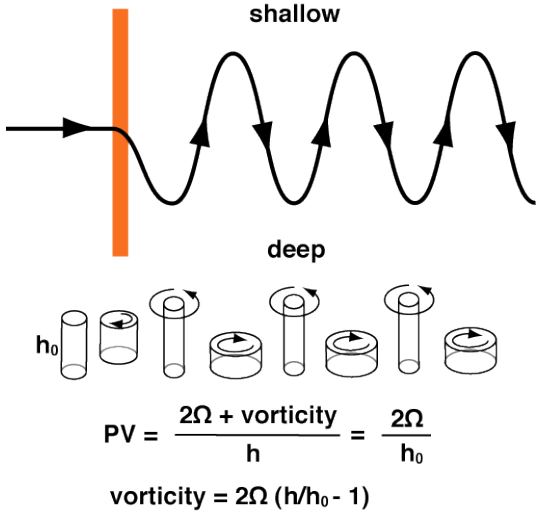

Figure 5.2. Illustration of the mechanisms that effect the PV and curvature of the flow, creating meanders (University of Chicago).

An additional fact that strengthens this theory is that the ARC flow velocity is higher at the segments between the various crests and troughs (Bower and Rossby 1989, Boebel 1999), thus illustrating

that the depth deviations not only affect the path of the ARC but also the speed of the current due to the conservation of mass .

The velocity is not the only parameter that is higher between the meandering features, meridional variance as calculated per each separate longitude is consistently lower at the peaks of the crests and troughs and higher in the segments in between them (with the exception of SC) (Figure 4.7). This implies that the sudden changes to the potential vorticity (ΔPV) which occur at set locations acts as a locking mechanism on the path of the current. Since the bottom topography does not significantly change (in the relevant time scales) the interaction with the current acts to reduce the positional variability.

5.2 ARC Meridional Variability

After discussing the stability of the quasi-stationary meanders, the stability of the mean latitudinal position of the ARC should be addressed. The anomalies of the mean latitudinal position fluctuate in the $\pm 0.4^{\circ}$ range but without any indication of a significant long term trend (Figure 4.5). A possible oscillation was identified with the use of spectral density analysis which revealed a signal in the semi-decadal frequency (Figure 4.6) however the data-set is not sufficiently long enough for the identification of more than one cycle. A gradual southward migration of approx. 0.55° was observed between 1994-2003 in the western section (Figure 4.5b) of the current followed by a northward trend that lasted for roughly the same period of time and with similar magnitude. While this pattern was still noticeable in the central section (Figure 4.5c), it was only statistically significant in the western section. No significant trends were identified in the eastern section (Figure 4.5d). Significant meridional shifts have been identified in the Kuroshio Current Extension during the mid 1980s and have been attributed to a 2° southward shift that was observed in the SST front of the Pacific SAFZ (Nakamura and Kazmin 2003). Similarly axial shifts in the Gulf Stream have been associated with the strengthening of the NAO (Joyce et al. 2000). The ARC displays a higher level of positional stability than the two aforementioned currents, this is possibly due to the stability of the ACC. Work done in the Southern Ocean (Boning et al. 2008) has shown that as a result of anthropogenic activity the ACC is becoming warmer and fresher, however, no increase in the tilt of the surfaces of equal density across the Antarctic Circumpolar Current has been detected. The study concluded that the meridional turnover in the Southern Ocean and the transport in the Antarctic Circumpolar Current are are insensitive to decadal changes in wind stress. A zonally averaged transport latitude index for the ACC shows no long-term trend, this implies that while meridional shifts do occur, large-scale changes in sea surface height are more likely to be

responsible for the localized shifts in frontal positions (Gille, 2014). This could explain why although regional intensification and warming have been documented for the ARC, no significant long term meridional trends have been observed. From 48° E and east-wards the ARC exhibits a predominantly south-ward trend (Figure 4.8), albeit a relatively small one, this could perhaps signify that the eastern section of the current is more susceptible to the wind stress variation and trends then the west region which is more topographically forced. As for why the western region of the ARC seems more susceptible to short term variations than either the central or eastern sections, this could be attributed to increased variability due to the regions proximity to the AC and Agulhas Retroflection region which are areas of high SSH variability. Although a single contributor that can explain the nature and direction of the anomalies from the mean latitudinal position has not been identified, the zonal characteristics of said anomalies hint that they may be associated to a regional factor i.e. AC transport anomalies or changes in the AR region. There is a noticeable northern anomaly peak circa 2013-2014 that might assist future work in identification of possible contributors to the variability.

5.3 EKE Seasonal Cycle

Wind stress is the primary source of kinetic energy in the ocean. Instabilities in global circulation result in the production of mesoscale eddies which slowly lose their energy through viscous dissipation and bottom friction. Oceanic kinetic energy is dominated by eddies, on average by a factor of 150 (Marshall and Plumb, 2007). While the major oceanic gyres span over vast regions, sub-sections within the gyre tend to follow a more localized seasonal cycle. The bi-modal distribution shown in Figure 4.9a indicates that EKE in the ARC follows a similar semi-annual seasonal cycle as does the South Indian Ocean Gyre. Work done on the seasonal circulation of the South Indian Ocean (Ffield, Toole and Wilson, 1997) have shown a maximum transport in the ARC during February-March and a minimum transport during June-July (Figure 5.3), this is consistent with our findings regarding the months with the maximum/minimum EKE values (Figure 4.10). The deviations from the mean transport (65 Sv.) range from +5 during summer to -10 during winter. These differences have been partially attributed to the meridional movement and strength of the SIOG. This strong decrease during June-July might explain why although regional winds have been shown to be on the rise, the increase in EKE during the summer period is significant while no significant increase to EKE has been observed during the winter months (Figure 4.13).

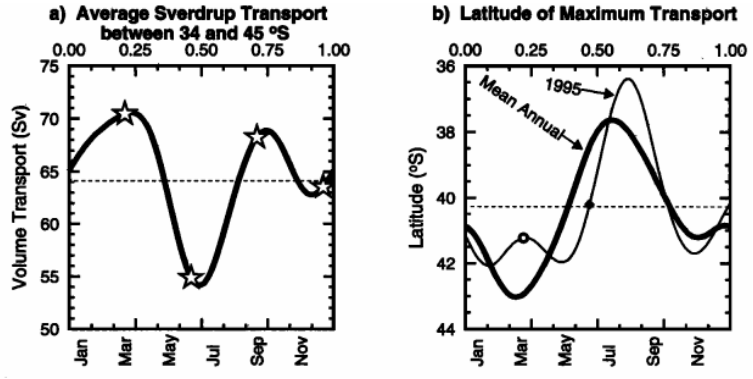

Figure 5.3 The mean annual Sverdrup transport between 34° and 45° S along 32.5° E, with stars marking the solstices and equinoxes (a). The mean annual curve of the latitude of maximum Sverdrup transport along 32.5° E, together with the 1995 curve displaying the occurrences of the March (open circle) and June (solid diamond) cruises. The data are smoothed by a 6 month gaussian filter, and the means are indicated by dashed lines (Ffield et al. 1997).

This finding is in line with recent discoveries by Scharrfenberg and Stammer (2010) who examined seasonal variations of the large-scale geostrophic flow field and eddy kinetic energy based on altimetric data. They revealed annual changes in all western boundary current systems due mainly to seasonally modulated strength changes in the Sverdrup circulation. In addition they found that, in the mid-latitudes, due to changes in the wind-driven barotropic circulation, the EKE field changes in its amplitude on the annual period, peaking in the summer. The spectral analysis conducted on the EKE time series indeed displays significant peaks in the semi-annual and annual frequencies (Figure 4.9b).

Our results indicating an increase in EKE, may also be related to the results produced in a recent study that showed that the Agulhas Current response to wind intensification is not in fact an increased flow but a broadening of the current as a result of increased eddy activity (Beal and Elipot, 2016). Similar studies (Yan et al. 2015; Cetina-Herdia et al. 2014) have hinted at similar trends in the KC and the East Australia Current providing further insight into how the ocean is responding to climate change.

There are various implications to increased regional eddy activity. One possible outcome is an increase to primary production. Geochemical estimates of production, based on calculations of heat fluxes and oxygen usage rates are double those found in biological samples. This is because biological measurements severely under-sample periodic nutrient injections into the photic zone. Eddy pumping represents one of the mechanisms for nutrient injection. The results from a study (Falkowski et al. 1991) investigating eddy enhanced primary production in a cyclonic gyre in the subtropical Pacific

reported that eddy pumping would enhance primary production by 20%. An additional study (Oschlies et al. 1998) that used a combination of remotely sensed SSH data from the TOPEX/Poseidon and ERS-1 satellite missions and a numerical eddy-resolving coupled ecosystem–circulation model of the North Atlantic Ocean demonstrated that mesoscale eddy activity can account for about one-third of the total flux of nitrate into the euphotic zone (a proxy for new production) in the subtropics and at mid-latitudes.

An additional implication to the increased eddy activity can be a varying effect on the regional carbon uptake. There are several parameters that affect the rates of CO_2 uptake by the ocean, most notably, biotic uptake, and solubility, the latter having more influence. Warm water can absorb less atmospheric carbon then cool water, therefore oceanic sinks are primarily regions where warm water cools down, such as WBC that bring warm water from lower warmer latitudes to higher cooler latitudes. The theoretic effect that the enhanced mixing might have on the CO_2 uptake varies between studies, some say that by strengthening vertical stratification in the high latitudes, mesoscale eddies can affect the rate at which the thermocline and intermediate waters are ventilated in addition to how water masses are transformed within the upper ocean (Lachkar et al.2007).

One particular matter on which many researchers seem to agree on is that when using models to help estimate global carbon uptake rates, the methods and resolutions in which the models resolve eddy activity greatly affects the outcome (Gnanadesikan, 2015; Ito, 2010; Orr, 2001). During the Ocean Carbon-Cycle Model Inter-comparison Project (OCMIP), several models were compared in order to try and identify major differences between them. One study concluded that horizontal eddy diffusion and parameterizations of isopycnal mixing as well as submesoscale eddies are crucial to modeling the carbon uptake. The choice of advection scheme for the model, which comes down to a trade-off between numerical precision and cost, is important with passive tracers such as anthropogenic CO_2 (Orr et al. 2001). Another study concluded that a better understanding of isopycnal mixing will be useful for generating projections of carbon feedbacks in the future. Resolving eddies requires resolutions of order 5 km which requires much more computational power than most models do (Gnanadesikan, 2015). Further research on the effects of eddy activity can help increase model precision and produce better model numerics that will allow us to better understand the biological and thermodynamic impacts of the changes in EKE we see in the ARC.

5.4 Inter-annual EKE variability

As shown in Figure 4.11, the variability of the EKE field over the ARC can be divided into

three regions. The reason that the western region (24°-40° E), the central region (40°-52° E) and the eastern region (52°-65° E) vary in values of variance is most likely due to several factors. The most notable of these are the vicinity of the region to the Agulhas Current and the Agulhas Retroflection area, levels of bathymetric influence and the interaction with neighboring currents i.e the ACC. Local peaks in variability are usually the result of baroclinic and barotropic instabilities generated by strong velocity gradients (Hakkinen and Rhines, 2009) such as those found in the AC and AR. Additional contributors to the EKE variability are Ekman pumping/suction (Qiu and Chen, 2010), wind forcing and frontogenesis (which is most prominent in areas with strong SST gradients like the ARC). The combination of the western region's vicinity to the AC and AR regions together with the relatively shallow depths and prominent bathymetric features that may enhance turbulence, lead it to be the highest in variability of the three. The loss of energy to dissipation and bottom friction leads to a decrease in variability throughout the central region. There is a slight increase in variability in the eastern region which indicates that the SWIR might be acting as an EKE dampener.

5.5 The Relationship Between SST, SSH and Atmospheric Pressure Anomalies

The IOSD describes the oscillation of SST anomalies in the subtropical Indian Ocean of which the positive phase is characterized by warmer sea surface temperatures in the southwestern part, south of Madagascar, and colder sea surface temperatures off Australia, this leads to higher precipitation levels in south and central Africa (Behara and Yamagata, 2001). The IOSD has been known to develop during December and January, peak in February and weaken by May-June (Behara and Yamagata, 2001). This is consistent with our findings regarding the ARC EKE seasonal cycle which has the highest mean values in February and lowest during July. The formation of the IOSD has been associated with wind intensification along the eastern area of the subtropical high, which in addition shifts slightly to the south during the event (Behara and Yamagata, 2001). Investigation of the lagging correlation between these events has led to the belief that it is the subtropical high pressure system that contributes to the formation of these SST anomalies and not the other way around. The IOSD has also been associated to a similar dipole in the southern Atlantic (Hermes and Reason, 2004) and to a lesser extent in the south-western Pacific indicating that these dipoles might be part of a larger-scale mode involving the southwestern parts of each ocean basin. Further support for this theory was provided via examination of the anomalies in the atmospheric circulation in the southern Indian and Atlantic Oceans, as the atmospheric pressure anomalies indicate a strengthening and a southward shift of the subtropical highs in both basins (Fauchereau et al. 2003). In an investigation regarding the relationship

between SST and SSH , correlations between the two fields ranged from 0.2-0.6 in most areas, however much higher correlations (˜0.7) where found in regions associated with ocean fronts and mesoscale variability (Jones, 1998). This interlocking relationship between SST anomalies, atmospheric pressure anomalies and EKE is consistent with our results showing a strong correlation between the EKE in the ARC and the IOSD index (Figure 4.15). The SAM is the leading mode of variability in the Southern Hemisphere atmospheric circulation on monthly and inter-annual timescales and therefore it is reasonable to conclude that the correlation found between the ARC EKE and the SAM index (Figure 4.14) has much to do with the effect SAM has on mid-latitude westerly winds.

5.6 Summary and Conclusions

Like other WBC extensions the path of the ARC is primarily forced by near-surface wind stress. However, on the mesoscale there is a lot of influence from the regional bottom topography. While not always clear from observations, due to the formation and transport of eddies, there are several topographically forced quasi-permanent meanders that characterize the flow path of the ARC. There is a lower variability of meridional position for the troughs and crests of these meanders than for the segments that connect between them. This implies that the interaction between the bathymetric features and the water mass which results in changes to the current's potential vorticity, causing the meanders, may be acting as a stabilizing mechanism that locks the current into its position.

While the western region of the current shows no long term trends the eastern region is predominantly south-bound. This may indicate that the western intensification and pole-ward shift that has been documented in the literature is manifesting mostly in the eastern section of the ARC which is less topographically bound. Another form of intensification that we are witnessing is an increase to the regional EKE, particularly during the summer when the EKE values peak. The implications of increased EKE are not fully understood but may include enhanced primary production and increased ocean-atmosphere interactions. Further exploring these implications may prove to be important for understanding the role of WBC and their extensions in the global carbon cycle. Understanding the role of vertical mixing in air-sea interaction is necessary for improving model calculations of heat flux and carbon exchange.

Analogous WBC extensions like the KE have been shown to migrate meridionally as a response to changes in either the main WBC (KC) or to other neighboring currents and fronts (in the case of the KE it was the SAFZ), the ARC's proximity to the ACC might however be acting as a stabilizing agent as it has been shown in the literature to be insensitive to long-term change. While no long-term

shifts have been identified, anomalies in the mean meridional position of the ARC show a possible north-south oscillation that can be primarily seen in the western most region of the current. A southward migration to the magnitude of approx. 0.55 ° from the mean current position occurred between 1993-2003, followed by a north-ward migration between 2003-2013.

The ARC EKE is linked to the SIOD indicating to a strong regional relationship between SSH and SST anomalies. The formation of the SIOD is attributed to shifts in the subtropical high pressure system, these shifts may be linking all of the subtropical regions of the Southern Hemisphere's three ocean basins. The SAM, which has been becoming increasingly positive in the past few years, may also be contributing to the regional EKE increase due to its association with the strengthening of the westerly winds.

With the world becoming increasingly warmer and with WBC's and their extensions having such a central role in transfering and spreading the heat, additional research into these worrying trends is crucial in order to better deal with the challenges facing us. The ARC is the largest source of EKE in the Indian Ocean in addition to acting as a major CO_2 sink, thus we recommend for further research to be conducted on this region. In particular, we recommend that further work should be done on improving how models resolve eddy activity in order to increase model accuracy in a region with increasing EKE. It's also important to further our understanding of the effects of increased eddy activity on primary production and ocean-atmosphere heat flux.

References

Alory, G., Wijffels, S., and Meyers, G. (2007). Observed temperature trends in the Indian Ocean over 1960-1999 and associated mechanisms. *Geophysical Research Letters*, 34(2):2–7.

Bader, J. and Latif, M. (2016). The impact of decadal-scale Indian Ocean sea surface temperature anomalies on Sahelian rainfall and the North Atlantic Oscillation. *Geophysical Research Letters*, 30(22).

Beal, L. M. and Elipot, S. (2016). Broadening not strengthening of the Agulhas Current since the early 1990s. *Nature*, 540(7634):570–573.

Behara, S. and Yamagata, T. (2001). Subtropical SST dipole events in the southern Indian Ocean. (2):1–3.

Boebel, O. and Barron, C. (2003). A comparison of in-situ float velocities with altimeter derived geostrophic velocities. *Deep Sea Research Part II: Topical Studies in Oceanography*, 50(1):119–139.

Boebel, O., Rossby, T., Lutjeharms, J., Zenk, W., and Barron, C. (2003). Path and variability of the Agulhas Return Current. *Deep-Sea Research Part II: Topical Studies in Oceanography*, 50(1):35–56.

Boebel, O., Schmid, C., and Zenk, W. (1999). Kinematic elements of Antarctic Intermediate Water in the western South Atlantic. *Deep Sea Research Part II: Topical Studies in Oceanography*, 46(1-2):355–392.

Böning, C. W., Dispert, A., Visbeck, M., Rintoul, S. R., and Schwarzkopf, F. U. (2008). The response of the antarctic circumpolar current to recent climate change. *Nature Geoscience*, 1(12):864–869.

Bower, A. S. and Rossby, T. (1989). Evidence of Cross-Frontal Exchange Processes in the Gulf Stream Based on Isopycnal RAFOS Float Data. *Journal of Physical Oceanography*, 19(9):1177–1190.

Chambers, D. P. (2018). Using kinetic energy measurements from altimetry to detect shifts in the positions of fronts in the Southern Ocean. *Ocean Science*, 14(1):105–116.

Chapman, C. C. (2014). Southern Ocean jets and how to find them: Improving and comparing common jet detection methods. *Journal of Geophysical Research: Oceans*, 119(7):4318–4339.

Combes, V. and Matano, R. P. (2014). Trends in the Brazil/Malvinas Confluence region. *Geophysical Research Letters*, 41(24):8971–8977.

Delman, A. S., McClean, J. L., Sprintall, J., Talley, L. D., Yulaeva, E., and Jayne, S. R. (2015). Effects of Eddy Vorticity Forcing on the Mean State of the Kuroshio Extension. *Journal of Physical Oceanography*, 45(5):1356–1375.

Deser, C., Alexander, M. A., and Timlin, M. S. (1999). Evidence for a Wind-Driven Intensification of the Kuroshio Current Extension from the 1970s to the 1980s. *Journal of Climate*, 12(6):1697–1706.

Dinezio, P. N., Clement, A. C., Vecchi, G. A., Soden, B. J., Kirtman, B. P., and Lee, S.-K. (2009). Climate Response of the Equatorial Pacific to Global Warming.

Dong, S., Hautala, S. L., and Kelly, K. A. (2007). Interannual Variations in Upper-Ocean Heat Content and Heat Transport Convergence in the Western North Atlantic. *Journal of Physical Oceanography*, 37(11):2682–2697.

Dong, S. and Kelly, K. A. (2003). Heat Budget in the Gulf Stream Region: The Importance of Heat Storage and Advection. Technical report.

Falkowski, P. G., Ziemann, D., Kolber, Z., and Bienfang, P. K. (1991). Role of eddy pumping in enhancing primary production in the ocean. *Nature*, 352(6330):55–58.

Fauchereau, N., Trzaska, S., Richard, Y., Roucou, P., and Camberlin, P. (2003). Sea-surface temperature co-variability in the southern Atlantic and Indian Oceans and its connections with the atmospheric circulation in the Southern Hemisphere. *International Journal of Climatology*, 23(6):663–677.

Ffield, A., Toole, J., and Wilson, D. (1997). Seasonal circulation in the South Indian Ocean. 24(22):2773–2776.

Friehe, C. A., Shaw, W. J., Rogers, D. P., Davidson, K. L., Large, W. G., Stage, S. A., Crescenti, G. H., Khalsa, J. S., Greenhut, G. K., and Li, F. (1991). Airâsea fluxes and surface layer turbulence around a sea surface temperature front. *Journal of Geophysical Research*, 96(C5):8593–8609.

Gille, S. T. (2014). Meridional displacement of the Antarctic Circumpolar Current. *Philosophical Transactions of the Royal Society A: Mathematical, Physical and Engineering Sciences*, 372(2019).

Gnanadesikan, A., Pradal, M.-A., and Abernathey, R. (2015). Isopycnal mixing by mesoscale eddies significantly impacts oceanic anthropogenic carbon uptake. *Geophysical Research Letters*, 42(11):4249–4255.

Goni, G. J., Bringas, F., and DiNezio, P. N. (2011). Observed low frequency variability of the Brazil Current front. *Journal of Geophysical Research*, 116(C10):C10037.

Gray, A. R. and Palter, J. B. (2017). *The role of western boundary current regions in the global carbon cycle*, volume 15.

Hakkinen, S. and Rhines, P. B. (2009). Shifting surface currents in the northern North Atlantic Ocean. *Journal of Geophysical Research*, 114(C4):C04005.

Hermes, J. C. and Reason, C. J. C. (2005). Ocean model diagnosis of interannual coevolving SST variability in the South Indian and South Atlantic Oceans. *Journal of Climate*, 18(15):2864–2882.

Huang, R. X., Russell, S., Huang, R. X., and Russell, S. (1994). Ventilation of the Subtropical North Pacific. *Journal of Physical Oceanography*, 24(12):2589–2605.

Ito, T., Woloszyn, M., and Mazloff, M. (2010). Anthropogenic carbon dioxide transport in the Southern Ocean driven by Ekman flow. *Nature*, 463(7277):80–83.

Jabaud-Jan, A., Metzl, N., Brunet, C., Poisson, A., and Schauer, B. (2004). Interannual variability of the carbon dioxide system in the southern Indian Ocean (20Â°S-60Â°S): The impact of a warm anomaly in austral summer 1998. *Global Biogeochemical Cycles*, 18(1):n/a–n/a.

Jones, S. (1998). Correlations between altimetric sea surface height and radiometric sea surface temperature in the South Atlantic Matthew Guymer 1 and Mark quantity dependent upon the temperature and salinity structure of the water column and on the depth independent baro. 103:8073–8087.

Joyce, T. M., Deser, C., and Spall, M. A. (1999). The Relation between Decadal Variability of Subtropical Mode Water and the North Atlantic Oscillation*. Technical report.

Kelly, K. A., Small, R. J., Samelson, R. M., Qiu, B., Joyce, T. M., Kwon, Y. O., and Cronin, M. F. (2010). Western boundary currents and frontal air-sea interaction: Gulf stream and Kuroshio Extension. *Journal of Climate*, 23(21):5644–5667.

Kwon, Y.-O., Alexander, M. A., Bond, N. A., Frankignoul, C., Nakamura, H., Qiu, B., Thompson, L. A., Kwon, Y.-O., Alexander, M. A., Bond, N. A., Frankignoul, C., Nakamura, H., Qiu, B., and Thompson, L. A. (2010). Role of the Gulf Stream and KuroshioâOyashio Systems in Large-Scale AtmosphereâOcean Interaction: A Review. *Journal of Climate*, 23(12):3249–3281.

Kwon, Y. O. and Deser, C. (2007). North Pacific decadal variability in the community climate system model version 2. *Journal of Climate*, 20(11):2416–2433.

Latif, M. and Barnett, T. P. (1994). Causes of Decadal Climate Variability over the North Pacific and North America. *Science*, 266(5185):634–637.

Levitus, S. (2000). Warming of the World Ocean. *Science*, 287(5461):2225–2229.

Liu, W. T., Xie, X., and Niiler, P. P. (2007). Ocean-atmosphere interaction over Agulhas Extension meanders. *Journal of Climate*, 20(23):5784–5797.

Lumpkin, R. and Garzoli, S. (2007). Interannual to decadal changes in the western South Atlantic's surface circulation.

Lutjeharms, J. R. and Ansorge, I. J. (2001). The Agulhas Return Current. *Journal of Marine Systems*, 30(1-2):115–138.

Marshall, G. J. (2003). Trends in the Southern Annular Mode from Observations and Reanalyses. *Journal of Climate*, 16(24):4134–4143.

Marshall, J. and Plumb, A. (2007). Circulation of the Atmosphere and Ocean: an introductory text. Technical report.

Matano, R. P. (1993). On the Separation of the Brazil Current from the Coast. *Journal of Physical Oceanography*, 23(1):79–90.

Metzl, N., Brunet, C., Jabaud-Jan, A., Poisson, A., and Schauer, B. (2006). Summer and winter airâsea CO2 fluxes in the Southern Ocean. *Deep Sea Research Part I: Oceanographic Research Papers*, 53(9):1548–1563.

Minobe, S., Kuwano-Yoshida, A., Komori, N., Xie, S. P., and Small, R. J. (2008). Influence of the Gulf Stream on the troposphere. *Nature*, 452(7184):206–209.

Nakamura, H. and Kazmin, A. (2003). Decadal changes in the North Pacific oceanic frontal zones as revealed in ship and satellite observations. *Journal of Geophysical Research*, 108(C3):3078.

Ohishi, S., Tozuka, T., and Komori, N. (2016). Frontolysis by surface heat flux in the Agulhas Return Current region with a focus on mixed layer processes: observation and a high-resolution CGCM. *Climate Dynamics*, 47(12):3993–4007.

Orr, J., Maier-Reimer, E., Mikolajewicz, U., Monfray, P., Sanniento, L., Toggweiler, J. R., Taylorfi, K., Sabine, L., and Qur, L. (2001). Estimates of anthropogenic carbon uptake from four three-dimensional global ocean models s Patrick Simulated global uptake agrees to within giving a range estimates of anthropogenic Column inventories of bomb become more similar to those for anthropogenic. *Global Biogeochemical Cycles*, 15(1):43–60.

Oschlies, A. and Garçon, V. (1998). Eddy-induced enhancement of primary production in a model of the North Atlantic Ocean. *Nature*, 394(6690):266–269.

P. Cetina-Heredia, Roughan, M., van Sebille, E., and Coleman, M. A. (2014). Journal of Geophysical Research Oceans. *Journal of Geophysical Research: Oceans*, (119):3868–3882.

Palmer, M. D., Bryden, H. L., Hirschi, J., and Marotzke, J. (2004). Observed changes in the South Indian Ocean gyre circulation, 1987-2002. *Geophysical Research Letters*, 31(15):2–5.

Peña-Molino, B. and Joyce, T. M. (2008). Variability in the Slope Water and its relation to the Gulf Stream path. *Geophysical Research Letters*, 35(3):L03606.

Pichevin, T. and Lutjeharms, J. (1999). Why Are There Agulhas Rings? Technical report.

Qiu, B. and Chen, S. (2010). Eddy-mean flow interaction in the decadally modulating Kuroshio Extension system. *Deep-Sea Research Part II: Topical Studies in Oceanography*, 57(13-14):1098–1110.

Qiu, B. O. (2003). Kuroshio Extension Variability and Forcing of the Pacific Decadal Oscillations: Responses and Potential Feedback. Technical report.

Rayner, N. A., Parker, D. E., Horton, E. B., Folland, C. K., Alexander, L. V., Rowell, D. P., Kent, E. C., and Kaplan, A. (2003). Global analyses of sea surface temperature, sea ice, and night marine air temperature since the late nineteenth century. *Journal of Geophysical Research*, 108(D14):4407.

Scharffenberg, M. G. and Stammer, D. (2010a). Seasonal variations of the large-scale geostrophic flow field and eddy kinetic energy inferred from the TOPEX/Poseidon and Jason-1 tandem mission data. *Journal of Geophysical Research*, 115(C2):C02008.

Scharffenberg, M. G. and Stammer, D. (2010b). Seasonal variations of the large-scale geostrophic flow field and eddy kinetic energy inferred from the TOPEX/Poseidon and Jason-1 tandem mission data. *Journal of Geophysical Research: Oceans*, 115(2):1–29.

Small, R. J., DeSzoeke, S. P., Xie, S. P., O'Neill, L., Seo, H., Song, Q., Cornillon, P., Spall, M., and Minobe, S. (2008). Air-sea interaction over ocean fronts and eddies. *Dynamics of Atmospheres and Oceans*, 45(3-4):274–319.

Stramma, L. and Lutjeharms, J. R. E. (1997). The flow field of the subtropical gyre of the South Indian Ocean. *Journal of Geophysical Research*, 102(15):5513–5530.

Taguchi, B., Xie, S.-P., Schneider, N., Nonaka, M., Sasaki, H., and Yoshikazu, S. (2007). Decadal Variability of the Kuroshio Extension : Observations and an Eddy-Resolving Model Hindcast. pages 2357–2377.

Talley, L. D., Pickard, G. L., Emery, W. J., and Swift, J. H. O. (2011). *Descriptive physical oceanography : an introduction*. Academic Press.

Tozuka, T. and Cronin, M. F. (2014). Role of mixed layer depth in surface frontogenesis: The Agulhas Return Current front. *Geophysical Research Letters*, 41(7):2447–2453.

Uenzelmann-Neben, G. (2002). Contourites on the Agulhas Plateau, SW Indian Ocean: indications for the evolution of currents since Palaeogene times. *Geological Society, London, Memoirs*, 22(1):271–288.

Wallace, J. M., Wallace, J. M., and Hobbs, P. V. (2006). *Atmospheric Science : an Introductory Survey*. Elsevier Science.

Wu, L., Cai, W., Zhang, L., Nakamura, H., Timmermann, A., Joyce, T., McPhaden, M. J., Alexander, M., Qiu, B., Visbeck, M., Chang, P., and Giese, B. (2012). Enhanced warming over the global subtropical western boundary currents. *Nature Climate Change*, 2(3):161–166.

Yan, X. and Sun, C. (2015). An altimetric transport index for Kuroshio inflow northeast of Taiwan Island. *Science China Earth Sciences*, 58(5):697–706.

Yang, H., Lohmann, G., Wei, W., Dima, M., Ionita, M., and Liu, J. (2016). Intensification and poleward shift of subtropical western boundary currents in a warming climate. pages 1–15.